CMS Draft Analysis Note

The content of this note is intended for CMS internal use and distribution only

2013/12/15
Head Id: 219929
Archive Id: 219897:219929M
Archive Date: 2013/12/08
Archive Tag: trunk

A Hadronic Search for Direct Stop with MT2 Variable Using the Full 2012 Data

Hamed Bakhshian[1], Shirin Chenarani[3], Esmaeel Eskandari[1], Ali Fahim[2], Abideh Jafari[1], Saeid Paktinat Mehdiabadi[1], and Maryam Zeinali[1]

[1] School of Particles and Accelerators, IPM, Tehran, Iran
[2] University of Tehran, Tehran, Iran, also at IPM
[3] Isfahan University of Technology, Isfahan, Iran, also at IPM

Abstract

A hadronic search for direct production of stops is performed on 20 fb^{-1} of data from proton-proton collision in the center of mass energy of 8 TeV at CMS. The most important backgrounds, are estimated using the data driven methods. It is shown that this analysis can access some parts of the SMS phase space which are not accessible by the E_T^{miss} analysis.

1 Introduction

Supersymmetry [1] (SUSY) is one of the most promising extensions of the Standard Model of the elementary particles (SM) which solves both the quadratic divergencies and hierarchy problems simultaneously. It introduces a new symmetry between the bosons and fermions and for every particle a sparticle is defined which is exactly the same, but differ in spin by 1/2. Since the super particles are not discovered yet, the supersymmetry should be a broken symmetry. Various mechanisms are introduced to break the symmetry softly without changing the other interesting features of the theory.

A search for new physics using 20 fb^{-1} of data from CMS taken in 2012 is documented in this note. Although the search is sensitive to any high scale new physics with a missing transverse momentum, R-parity conserving SUSY model is used to illustrate the performance of the method.

The search variable is the stransverse mass (M_{T2}) which is the natural extension of the known transverse mass (m_T) to a case when two massive particles with equal mass are created in pairs and decay via a chain of jets and leptons to two invisible particles. In the case of R-Parity conserving SUSY, the Lightest Supersymmetric Particle (LSP) escapes the detection and appears as a missing transverse momentum. The distribution of M_{T2} reflects the scale of the produced particles and is much higher for sparticles compared to the SM particles. Hence, SUSY should appear as an excess in the tail of the M_{T2} distribution. It was shown previously [2] that M_{T2} is a powerful variable to search for SUSY. Due to consistency of the data with background only hypothesis, low mass gluino and squarks have been ruled out. A main direction suggested by the theoreticians and phenomenologists is to search for the third generation of the sparticles. Since the third generation of the SM particles are heavier than the first two generations, in the SUSY sector, this generation can be much lighter. The current analysis is optimized to search for the direct production of the supersymmetric partner of the top quark (stop) in the hadronic final states. It is assumed that the pair produced stops undertake the following decay chain:

$$\tilde{t} \rightarrow t + \tilde{\chi}_1^0 \tag{1}$$

when top decays hadronically:

$$t \rightarrow b + W \rightarrow b + q + q' \tag{2}$$

and $\tilde{\chi}_1^0$ can not be detected and appears as missing transverse momentum (E_T^{miss}).

The previous version of the analysis which used only 5.1 fb^{-1} of 2012 data was documented in another analysis note [3]. In this version, the full 2012 data is used and some parts of the analysis have been modified.

After introduction in the next section the M_{T2} variable is introduced. A sepcial method for top reconstruction is described in section 3. The data and MC samples are defined in section 4. Different physical objects used in this analysis are introduced in section 5. Sections 6-7 review the procedure to select the trigger and cuts to have a better reach in this search. Our strategy to search for stop is explained in section 8. Data driven methods are used to estimate the contribution of the main SM backgrounds. Section 9 shows the methods and their performance. The statistical methods are used to interpret the results in section 10 and finally section 11 concludes the note.

2 The definition of $\mathbf{M_{T2}}$

The variable transverse masss is used to measure the mass of the W-boson [4–7] in its decay to a lepton and a neutrino, where only the transverse missing energy due to undetected neutrino could be measured. It is defined as

$$m_T^2 = 2\,(E_T^l E_T^\nu - \vec{p_T}^{\,l}.\vec{p_T}^{\,\nu}), \tag{3}$$

where for neutrino, $E_T^\nu = p_T^\nu$. The kinmatic endpoint of m_T is an estimator for the W-mass, i.e. $m_T^2 \leq m_W^2$.
The M_{T2} variable [8, 9] is introduced and used in this analysis to discriminate between SUSY signal and the SM backgrounds while it is originally intended to estimate the mass of unseen particles. The kinematic endpoint of M_{T2} carries model independent information about the mass difference between the primary and the secondary supersymmetric particles. It is in particular useful to study events containing two simultaneous decays of a supersymmetric particle into a visible and an undetectable particle (e.g. neutralino). It is defined as

$$M_{T2}(m_\chi) = \min_{p_T^{\chi_1}+p_T^{\chi_2}=E_T^{miss}} \left[\max\left\{\, m_T(p_T^{\chi_1}; m_\chi),\, m_T(p_T^{\chi_2}; m_\chi)\,\right\}\right], \tag{4}$$

where χ stands for the neutralino whose mass is a free parameter in the evaluation of M_{T2}. The choice of maximum m_T is reasonable since none of the two transverse mass exceeds the mass of parents. The chosen transverse mass is minimized over the range of m_χ which again ensures that m_T is less than the parents mass.
While for boosted systems in the transverse plain M_{T2} can be computed only numerically, there are analytic solutions [10] for unboosted scenarios. There, one can write the M_{T2} endpoint as a function of the masses.
To reconstruct the visible system as the input for M_{T2} calculation, the visible part of the event (jets in this analysis) is decomposed into two *pseudojets*. The procedure is known as *hemisphere* reconstruction and is already used in [11]. The two massless jets with the highest invariant mass define the primary two directions of hemispheres. Other jets are added to one of the hemispheres based on the minimal Lund distance (see e.g. [12]). The resulting M_{T2} variable is proven to well reject the multi-jet processes with non-genuine E_T^{miss} [11].

3 Top Reconstruction

To reconstruct top quarks a special method is used. The main features of the method are using a χ^2 and mass of the jets. A χ^2 is constructed based on the known masses of W and top, e.g.

$$\chi^2 = \frac{(M_{2j} - M_W)^2}{\sigma_W^2} + \frac{(M_{3j} - M_t)^2}{\sigma_t^2}; \tag{5}$$

M_{2j} is usually the invariant mass of 2 jets making a W boson, but it can also be a heavy single jet. The uncertainty on invariant masses is computed as

$$\sigma_x = \sqrt{\frac{1}{4}\sum_i \quad (\frac{\Delta p_i}{p_i})^2 \quad (\frac{\sum_{j\neq i} M_{ij}^2}{M})^2 + \Gamma_x^2}; \tag{6}$$

where p_i uncertainty is taken as $\frac{\Delta p_i}{p_i} = \frac{100\%}{\sqrt{p_i}}$ and Γ_x is the width of W (2.1 GeV) and top (10 GeV). Top reconstruction is started by reconstructing all possible W's from either 2 jets (W2j) or

1 heavy jet (W1j). Solutions are kept only if they have a χ^2 which is less than a fixed maximum value (2 in this analysis) for W in W2j and in W1j giving the W mass in a small window ($80.4 \pm 10.0\ \mathrm{GeV}/c^2$). To calculate the χ^2 for W1j, the width (Γ_x) in Equation 6 is set equal to $10\ \mathrm{GeV}/c^2$. If a heavy jet is in a given mass range and is b-tagged, it is considered as a coalescence of a b with a jet from W (W1b). The mass window for W1b is set to [40,130] GeV/c^2 . $\chi^2 = 1$ is assigned to W1b candidates to avoid any systematically decrease of χ^2 for the top combinations containing such objects. All reconstructed W's are ordered in their χ^2 value. In case of overlapping W's, only the best χ^2 solution is kept. In the next step, the reconstructed W's are used to reconstruct the top candidates by adding a free jet. To reduce the correlations, before using the W's, their 4-vector is rescaled to give the correct W mass ($80.4\ \mathrm{GeV}/c^2$). If there is any overlap between the tops, the combination with a correct b-tagged jet (b+W) or a W1b is preferred over the best χ^2 solution.

3.1 Performance of the Algorithm

By efficiency we want to know how many of generated top quarks are found at reconstruction level with the top search algorithm. Only hadronically decaying top quarks are considered. Efficiency is defined as

$$\epsilon_{topSearch} = N^{matched}_{reco-top} / N^{hadronic}_{gen-top}$$

where reconstructed top quarks are matched with generated ones if $\Delta R(top_{rec}, top_{gen}) < 0.1$. The overall results are shown in Table 1.

#events	#gen-top-hadronic	#rec-top-all	#rec-top-matched	Overall efficiency
1.16 ME	2601	1331	936	36%

Table 1: The total efficiency of the top reconstruction algorithm. The efficiency is defined as the fraction of the generated top quarks which are reconstruted by the top search algorithm.

Efficiency versus different event kinematic variables is studied and the results are shown in Figure 1. Efficiency is investigated in different jet bins. The probability to find a hadronically decaying top is higher in higher jet multiplicities.

The efficiency of the top reconstruction vs. number of b-tagged jets is also studied. Although there is no constraint for the combination to contain a b-tagged jet, in case of a tagged jet in the top combination, it is preferred over minimum χ^2. Efficiency is stable in Nb-jets bins, as expected. The last bin suffers from low statistics.

As the efficiency versus the top p_T is shown in Figure 1, if top quarks are generated with higher p_T, there is a higher probability for them to be reconstructed by our algorithm.

This study shows that efficiency is stable in M_{T2} bins, apart from the last two bins which have few entries.

The fake rate of the top reconstruction algorithm is also studied. Fake Rate, can be defined as the Probability of reconstructing top from each 3 jets in a W + jets event. So the ratio is normalized to the number of jets. The results after applying all MT2b cuts on the WJetsToLNu-HT-400ToInf-8TeV sample are shown in Figure 2. The studies show that the fake rate value is around 20%.

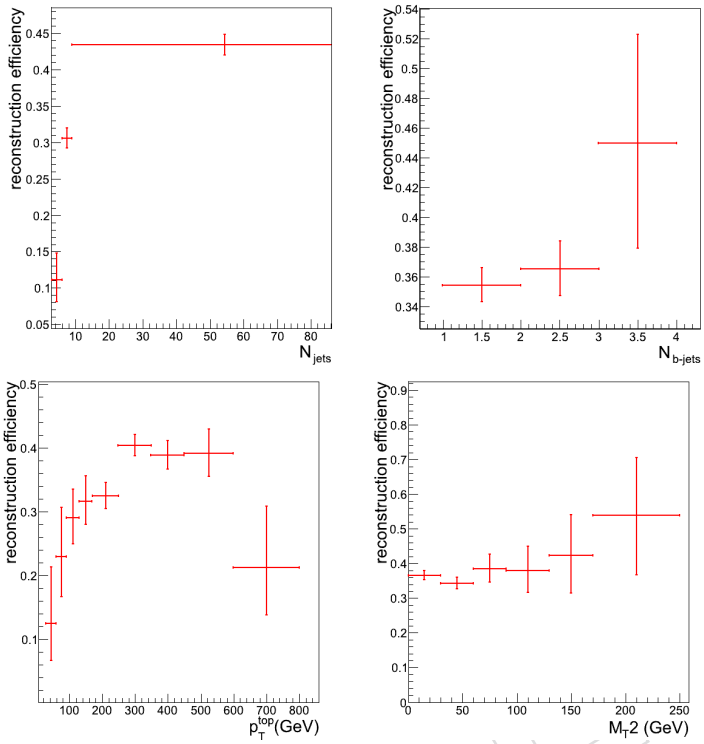

Figure 1: The efficiency of top quark reconstruction algorithm is shown vs. number of jets (top-left) and number of b-tagged jets (top-right), top p_T (bottom-left) and M_{T2} and (bottom-right).

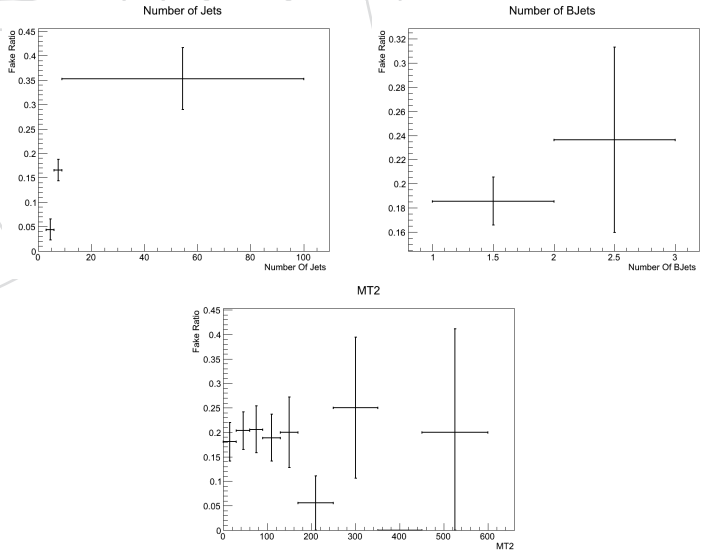

Figure 2: The fake rate of the top reconstruction algorithm is shown vs. number of jets (top-left), number of b-tagged jets (top-right) and M_{T2} (bottom).

4 Datasets and MC samples

To reconstruct the objects, the CMSSW_5_3_7_patch5 is used for both data and MC. The data used in the analysis corresponds to 19.6 fb^{-1} of proton-proton collisions in the center of mass energy of $\sqrt{s}$ = 8 TeV which was taken in 2012. The list of the datasets, the run range and the corresponding integrated luminosities are as follow:

- /MultiJet/Run2012A-13Jul2012-v1/AOD (190456-193621, 952.6 pb^{-1})
- /MultiJet/Run2012A-recover-06Aug2012-v1/AOD (190782-190949, 95.4 pb^{-1})
- /MultiJet/Run2012B-13Jul2012-v1/AOD (193834-196531, 4.94 fb^{-1})
- /MultiJet/Run2012C-24Aug2012-v1/AOD (198022-198523, 520.4 pb^{-1})
- /MultiJet/Run2012C-PromptReco-v2/AOD (198941-203742, 6.9 fb^{-1})
- /MultiJet/Run2012D-PromptReco-v1/AOD (203777-208686, 7.7 fb^{-1})

Only the lumisections with fully operative CMS subdetectors are used in this analysis (golden JSON files). To optimize the search method, MC samples are used for different Standard Model backgrounds and signals. These samples are officially generated and reconstructed by the CMS collaboration. The full list of the samples and their cross sections are given in Table 2. For most of the samples the most accurate calculation of the cross sections available in the literature (usually NLO) are used.

5 Physics Object Definition and Preselections

This section, describes the physics objects used in this analysis.

5.1 PF Jets

- PF jets with $p_T > 20$ GeV and $|\eta| < 2.4$ are kept for the analysis.
- Jets are required to pass loose pf-jet id cuts listed below:
  - Number of constituents > 1,
  - Neutral hadronic fraction < 0.99,
  - Neutral electromagnetic fraction < 0.99,
  - Charged hadronic fraction > 0,
  - Charged electromagnetic fraction < 0.99,
  - Charged multiplicity > 0.

5.2 PF Electrons

- PF electrons with $p_T > 10$ GeV and $|\eta| < 2.4$ are selected with ECAL gap veto.
- Electrons are required to pass cut-based electron id cuts corresponding to VBTF 95 working point, which is used for veto [13]. These set of cuts contain the requirements on $|d0| < 0.04$ cm and $|dz| < 0.2$ cm, for which both of them are calculated with respect to the primary vertex.
- Combined relative PF isolation below 0.15.

5.3 PF Muons

- PF muons with $p_T > 10$ GeV and $|\eta| < 2.4$ are selected, which are asked to be global muons.

Table 2: List of the MC samples used in this analysis.

Sample name	σ (pb)
QCD	
QCD-Pt-120to170-TuneZ2star-8TeV-pythia6-Summer12-DR53X-PU-S10-START53-V7A-v3	156293.3
QCD-Pt-170to300-TuneZ2star-8TeV-pythia6-v2-...-v1	34138.15
QCD-Pt-300to470-TuneZ2star-8TeV-pythia6-v3-...-v1	1759.55
QCD-Pt-470to600-TuneZ2star-8TeV-pythia6-...-v2	113.88
QCD-Pt-600to800-TuneZ2star-8TeV-pythia6-...-v2	26.99
QCD-Pt-800to1000-TuneZ2star-8TeV-pythia6-...-v2	3.55
QCD-Pt-1000to1400-TuneZ2star-8TeV-pythia6-...-v1	0.74
QCD-Pt-1400to1800-TuneZ2star-8TeV-pythia6-...-v1	0.034
QCD-Pt-1800-TuneZ2star-8TeV-pythia6-...-v1	0.0018
Top	
TTJets-MassiveBinDECAY-TuneZ2star-8TeV-madgraph-tauola-Summer12-DR53X-PU-S10-START53-V7A-v1	234
T-t-channel-TuneZ2star-8TeV-powheg-tauola-...-v3	47
Tbar-t-channel-TuneZ2star-8TeV-powheg-tauola-...	25.00
T-tW-channel-DR-TuneZ2star-8TeV-powheg-tauola-...	10.7
Tbar-tW-channel-DR-TuneZ2star-8TeV-powheg-tauola-...	10.7
T-s-channel-TuneZ2star-8TeV-powheg-tauola-...	2.82
Tbar-s-channel-TuneZ2star-8TeV-powheg-tauola-...	1.57
WJets	
WJetsToLNu-HT-250To300-8TeV-madgraph-v2-Summer12-DR53X-PU-S10-START53-V7A-v1	48.01
WJetsToLNu-HT-300To400-8TeV-madgraph-v2-...	38.3
WJetsToLNu-HT-400ToInf-8TeV-madgraph-...	25.22
WJetsToLNu-HT-200To250-8TeV-madgraph-...v1-2	90.27
ZJets	
DYJetsToLL-M-10To50filter-8TeV-madgraph-...Summer12-DR53X-PU-S10-START53-V7A-v1	876.8
DYJetsToLL-M-50-TuneZ2Star-8TeV-madgraph-tarball- ...	3503.71
ZJetsToNuNu-50-HT-100-TuneZ2Star-8TeV-madgraph-ext-...	381.2
ZJetsToNuNu-200-HT-400-TuneZ2Star-8TeV-madgraph-ext-...	41.49
ZJetsToNuNu-400-HT-inf-TuneZ2Star-8TeV-madgraph-ext-...	5.27
ZJetsToNuNu-100-HT-200-TuneZ2Star-8TeV-madgraph-ext-...V7C-v1	160.3
SMS	
SMS-T2tt-mStop-150to350-mLSP-0to250-8TeV-Pythia6Z-Summer12-START52-V9-FSIM-v1-2	
SMS-T2tt-mStop-375to475-mLSP-0to375-8TeV-Pythia6Z-...	
SMS-T2tt-mStop-500to650-mLSP-0to225-8TeV-Pythia6Z-...	
SMS-T2tt-mStop-500to650-mLSP-250to550-8TeV-Pythia6Z-...	
SMS-T2tt-mStop-675to800-mLSP-0to275-8TeV-Pythia6Z-...	
SMS-T2tt-mStop-675to800-mLSP-300to700-8TeV-Pythia6Z-...	

- Normalized χ^2 is required to be below 10.
- At least one valid track hit and at lease one valid pixel hit is required.

- Number of chambers with matched segments is required to be greater than one and number of silicon layers should be above 5.
- Cuts on the $|d0| < 0.2$ cm and the $|dz| < 0.5$ cm, both with respect to the primary vertex, are applied.
- Combined relative PF isolation below 0.2.

5.4 PF Taus

In this note taus always mean hadronically decaying taus, unless stated otherwise.

- Hadron Plus Strip (HPS) algorithm identified PF-taus
- $p_{\mathrm{T}} > 20$ GeV and $|\eta| < 2.3$
- A decay into one or three prongs, plus eventually a π^0, is required
- Loose Electron Rejection: electron pion MVA discriminator < 0.6
- Tight Muon Rejection: Tau Lead Track not matched to chamber hits, and no DT, CSC or RPC Hits in last 2 stations, and large enough energy deposit in ECAL + HCAL in 1 prong + 0 strip decay mode ($\sum$(ECAL+HCAL) $> 0.2 \cdot p_{\mathrm{T}}$.
- Loose Isolation ($\Delta\beta$-corrected): $\Delta\beta$-corrected $\sum p_{\mathrm{T}}$ of PF charged and PF gamma isolation candidates ($p_{\mathrm{T}} > 0.5$ GeV) less than 2 GeV (in a cone of $\Delta R = 0.3$ around the tau axis), requiring 3 hits on tracks of charged isolation candidates.

5.5 PF E_T^{miss}

- Type1 corrected PF E_T^{miss} is used.

5.6 Jet/MET Smearing

Simulated events show discrepancies with data specially in E_T^{miss} and M_{T2} distributions. As shown in Figure 3, the data over MC shows a trend rather than fluctuating differences.

The energy of jets and E_T^{miss} in simulation are calibrated based on data. There are however

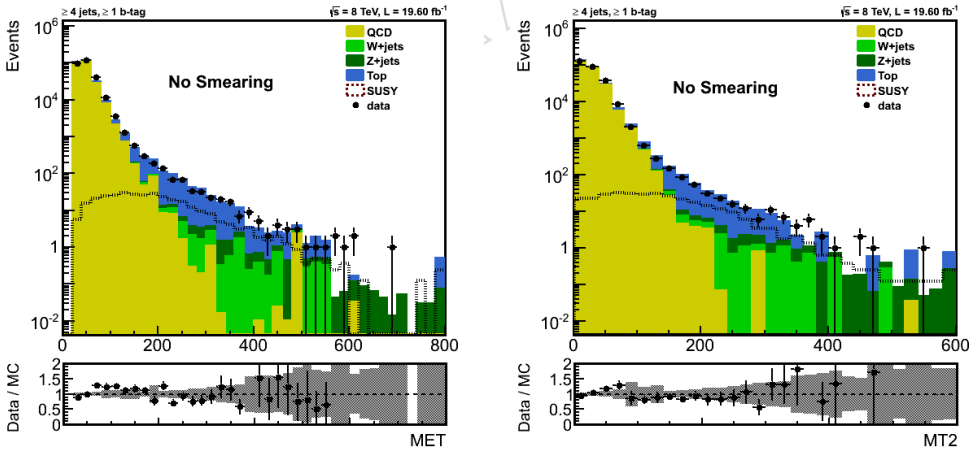

a b

Figure 3: The distribution of E_T^{miss} (a) and M_{T2} (b) before smearing.

residual differences between data and simulation which are not covered by those corrections. Such differences could be improved by altering the jet energy resolution to match the data

and correcting the E_T^{miss} accordingly. The CMS official recipe is followed to for the jet-E_T^{miss} smearing. Figure 4 illustrates the improvement achieved after smearing in E_T^{miss} and M_{T2} distributions. Smeared jets and E_T^{miss} are used in event selection and in the rest of the analysis.

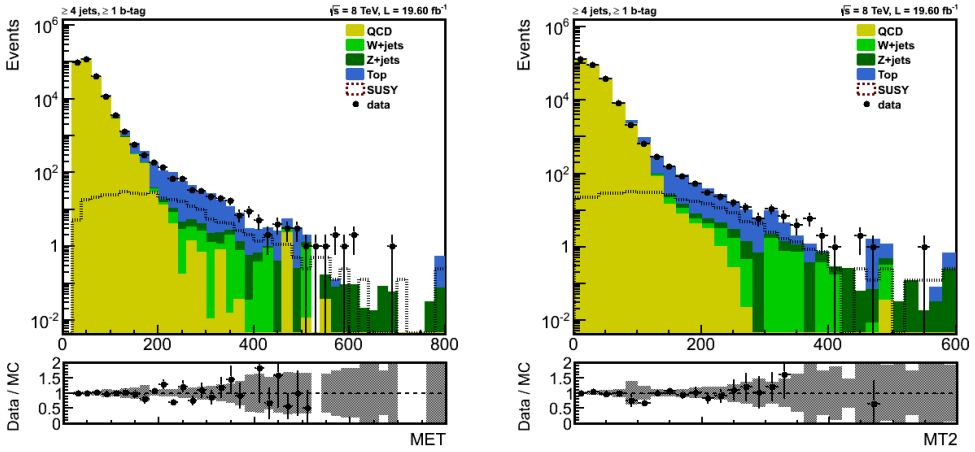

a b

Figure 4: The distribution of E_T^{miss} (a) and M_{T2} (b) after smearing.

5.7 Preselection

- At least one good vertex, with $\rho < 2$ cm and $|z| < 24$ cm and Ndof > 4 is requested.
- There are some cleaning cuts which are applied against instrumental effects, including those listed below:
  - An isolation based HBHE noise filter is applied,
  - Events identified as beam halo are filtered.

5.8 MT2b Cuts

This section provides a review on the cuts which are started with to study the triggers. This set of cuts are those mainly used in the MT2b analysis [2]. Once the trigger is fixed, the optimized set of selection cuts which are used in the main stream of the current analysis will be described in detail in Section 7.

- The preselection cuts which was outlined in Section 5.7.
- At least 4 jets with $p_T > 40$ GeV and $|\eta| < 2.4$ are required which are asked to pass loos pf-jet id cuts.
- The leading jet-p_T should be greater than 150 GeV.
- It is also required that all jets with $p_T > 50$ GeV to pass loose pf-jet id cuts. Events with non-idetified high p_T jets are discarded.
- At least one b-quark jet is requested with $p_T > 20$ GeV within the tracker acceptance, which is tagged by the Simple Secondary Vertex algorithm with a tight working point.
- The difference between E_T^{miss} and the vectorial p_T sum of the selected jets, electrons and muons, hereafter referred to as VectorSumPt, should be below 70 GeV.

- E_T^{miss} is required to be greater than 30 GeV.
- The minimum $\Delta\phi$ between E_T^{miss} and the four leading jets, hereafter referred to as $\Delta\phi_4^{min}$, should be greater than 0.3. There is no requirement on the id or p_T of the jets when looking for the minimum azimuthal angle between E_T^{miss} and jets.
- A cut on $M_{T2} > 125$ GeV is applied.
- Leptons, being either electrons or muons, are vetoed.

6 Trigger

6.1 Trigger Study

To have the best reach, two sets of triggers are compared. Their names and run ranges are shown in table 3. The corresponding prescaled triggers which are used to find the trigger plateau are also shown.

Table 3: On line triggers, their references and run ranges. A logical OR between SixJet and QuadJet is used.

HT		
Trigger Path	Prescaled Trigger	Run Range
HLT_PFHT650_v5	HLT_PFHT350_v3	190650-190750
HLT_PFHT650_v6	HLT_PFHT350_v4	191000-191400
HLT_PFHT650_v7	HLT_PFHT350_v5	191500-193750
HLT_PFHT650_v8	HLT_PFHT350_v6	193750-196030
HLT_PFHT650_v9	HLT_PFHT350_v7	196046-196531
MultiJet		
HLT_SixJet45_v1	HLT_SixJet35_v1	190456 - 190738
HLT_SixJet45_v2	HLT_SixJet35_v2	190782 - 196027
HLT_SixJet45_v3	HLT_SixJet35_v3	196046 - 196531
HLT_QuadJet80_v1	HLT_QuadJet70_v1	190456 - 190738
HLT_QuadJet80_v2	HLT_QuadJet70_v2	190782 - 196027
HLT_QuadJet80_v3	HLT_QuadJet70_v3	196046 - 196531

To take into account the statistics (the peak of the selected events by the un-prescaled trigger figure 5 (middle)), we look at the efficiencies bin-by-bin and distribution of efficiencies (un-prescaled divided by the prescaled, figure 5 (right)) with different HT cuts are weighted according to the statistics of the un-prescaled histogram. The cut that gives the mean value greater than 95% is chosen as the offline cut on the trigger parameter. An example of this method for different cuts on the HT for HLT_PFHT650_vX is shown in figure 6.

The result of this method is HT > 700 GeV, but we use 725 GeV conservatively. For the multijet triggers, same method is used and depending on the number of jets different cuts on the P_T of the jets are found. The result is summarized here:

- HLT_SixJet45_vX, 6 jets with $p_T > 65$ GeV/c or 7 jets with $p_T > 55$ GeV/c
- HLT_QuadJet80_vX, 4 jets with $p_T > 100$ GeV/c or 5 jets with $p_T > 85$ GeV/c

As another possibility, one can think of decreasing the number of jets and increasing the p_T threshold, but it does not reach the plateau and is excluded from the list. Asking for 7 jets means that we rely on ISR/FSR and it is not safe in the systematic point of view, the increase of

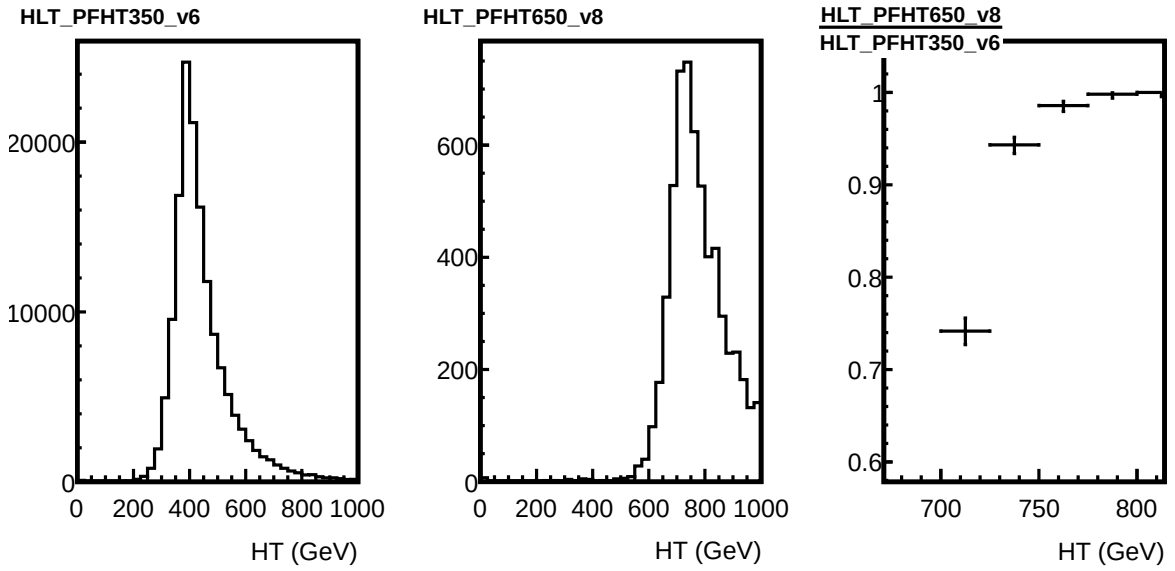

Figure 5: The prescaled (left) and un-prescaled (middle) HT triggers. The right plot shows the ratio of the two previous histograms zoomed in the interesting part.

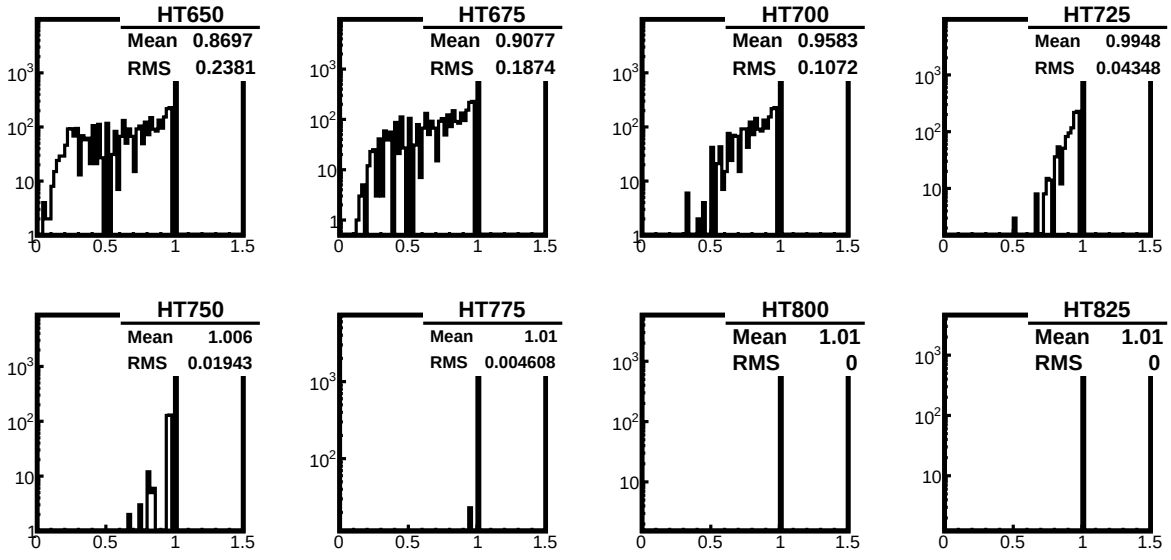

Figure 6: The weighted mean of the efficiencies in figure 5(right) for different cuts on HT. HT $>$ 700 GeV gives 95% efficiency.

the yield due to adding this cut is negligible (606 events in data increases to 615), so this part is dropped from the offline cuts.

After increasing the statistics to 20 fb^{-1}, the following online triggers with the same offline triggers are added to the analysis.

6.2 Trigger Selection

To investigate the efficiency of different trigger sets the SMST2tt sample is used. The selection cuts described in section 5.8 are applied on top of the trigger selection. The ratio of the signal events passing all the cuts is shown for two different sets of triggers as a function of $\tilde{t}$ mass

Table 4: On line triggers and run ranges. A logical OR between SixJet and QuadJet is used.

HLT_SixJet45_v4	198022 - 199608
HLT_SixJet45_v6	199698 - 209151
HLT_QuadJet80_v4	198022 - 199608
HLT_QuadJet80_v6	199698 - 209151

and $\tilde{\chi}_1^0$ mass in figure 7. Although the signal efficiency is ~ 4 times larger when the HT trigger is used, MC studies show that the number of remaining backgrounds are so larger that the multi-jet trigger is more powerful to exclude. The estimated exclusion power of both triggers are compared in figure 8.

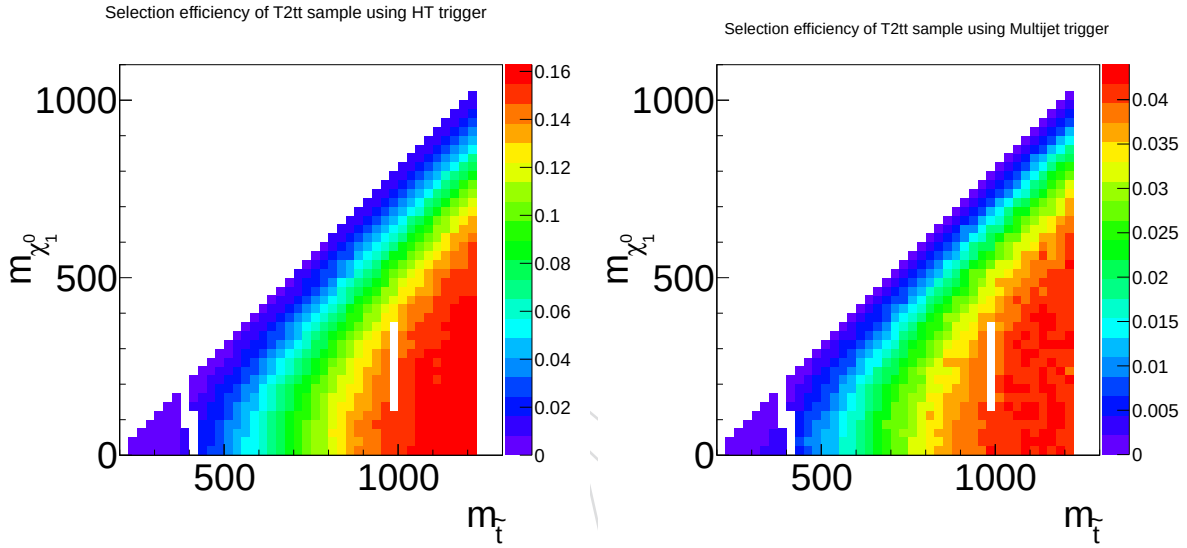

Figure 7: The efficiency of different trigger sets (Left : HT trigger, Right : Multijet trigger) for the SMST2tt sample. The results are shown as a function of the $\tilde{t}$ mass and $\tilde{\chi}_1^0$ mass.

7 Selection Cuts

In order to select signal events and suppres SM backgrounds, a set of cuts which are listed below, is applied.

- The preselection cuts which was outlined in Section 5.7.
- Offline trigger cuts mentioned in Section 6.1. They ask for at least 4 jets with $|\eta| < 2.4$
- Among these set of jets, first and second leading jets are needed to have a p_T greater than 100 GeV and 60 GeV, respectively.
- It is also required that each jet with $p_T > 50$ GeV to pass loose pf-jet id cuts.
- At least one b-quark jet is requested with $p_T > 20$ GeV within the tracker acceptance, which is tagged by the Combined Secondary Vertex algorithm with a tight working point.
- The difference between E_T^{miss} and the vectorial p_T sum of the selected jets, electrons and muons should be below 70 GeV.
- The $\Delta\phi_4^{min}$ of the four leading jets should be greater than 0.3. There is no requirement

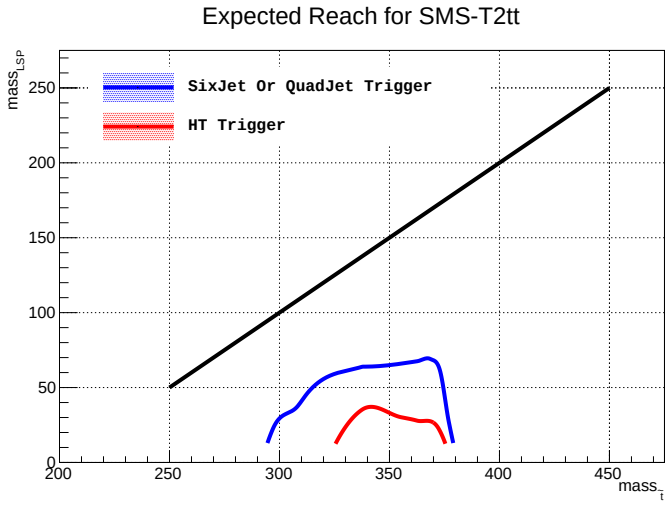

Figure 8: The estimated exclusion power for two different sets of triggers. The multijet trigger is used in this analysis.

on the id or p_T of the jets when looking for the minimum azimuthal angle between E_T^{miss} and jets.

- E_T^{miss} is required to be greater than 30 GeV.
- Leptons, being either electrons or muons, are vetoed.
- A cut on $M_{T2} > 125$ GeV is applied.

The effect of the selection cuts on different backgrounds is shown is Table 5

Cut	QCD	W+jets	Z+jets	Top	Total
Trigger	5715523.28	7307.79	2432.95	60071.28	5785335.30±26646.27
Jet ID	5713982.08	7292.60	2432.95	60040.64	5783748.26±26645.46
Lepton Veto	5709941.35	4759.89	1855.46	51143.85	5767700.56±26642.92
BJet	583250.20	323.93	155.37	34252.57	617982.07±8690.65
$\Delta\phi_4^{min} > 0.3$	310092.56	198.38	103.58	19147.93	329542.46±6437.28
$M_{T2} > 125$	465.73	30.99	22.92	561.55	1081.19±121.23
$\mid E_T^{miss} - MHT \mid < 70$	72.22	27.66	20.47	470.25	590.61±21.63

Table 5: Event yields after applying different cuts. "Trigger" contains all of the preselections and offline trigger cuts.

7.1 Cuts Justification

We performed some checks to justify our analysis cuts. Our cuts were optimised based on maximization of the statistical significance. We studied our main cuts in this analysis. In Figure 9 we show the M_{T2} distribution for QCD for different intervals of VSPT. The different distributions are normalized to the same area. The variable is plotted for QCD events that pass the cuts described above. From Figure 9, we see that for large values of VSPT, the M_{T2} distribution is distorted and deviates from the distribution with $0 <$ VSPT < 20, i.e. small VSPT. Since the distortion becomes significant for VSPT > 70 GeV, we cut away events above this value.

We looked at the distributions of different variables before and after applying VSPT < 70 when the other cuts except $M_{T2} > 125$ were relaxed. As it is obvious from Figures 10-15, by applying VSPT < 70 we have better agreement between data and MC,

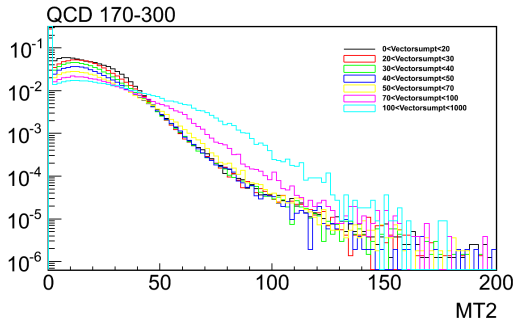

Figure 9: Disrtibution of M_{T2} in different VSPT ranges for one QCD sample

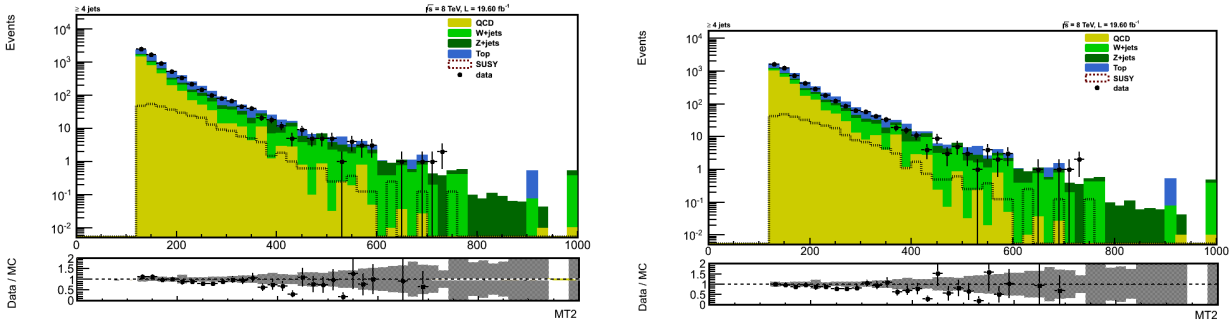

(a) (b)

Figure 10: Distribution of M_{T2} before(a) and after(b) applying VSPT < 70

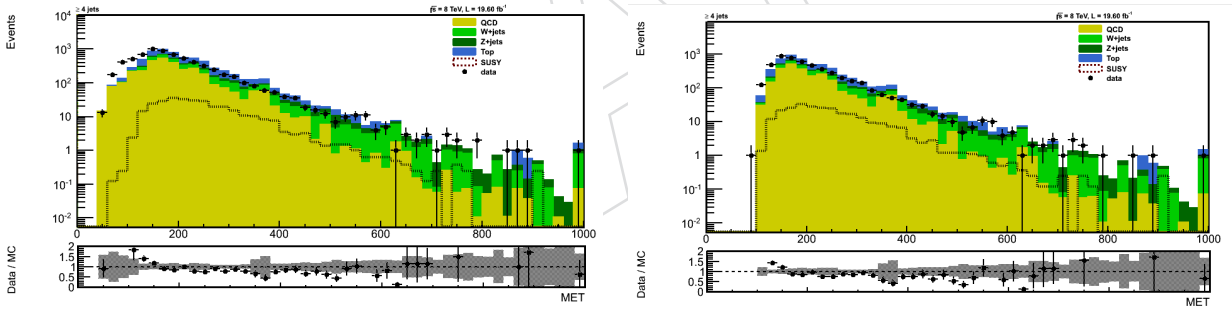

(a) (b)

Figure 11: Distribution of E_T^{miss} before(a) and after(b) applying VSPT < 70

To justify the cut on $\Delta\phi_4^{min}$ which is $\Delta\phi_4^{min} > 0.3$, like VSPT, We looked at the distributions of different variables before and after applying $\Delta\phi_4^{min} > 0.3$ when the other cuts except $M_{T2} > 125$ were relaxed. As it is obvious from figures 16-21, by applying $\Delta\phi_4^{min} > 0.3$ we have a better agreement between data and MC,

We applied Jet-Met smearing on MC samples and then plotted the distributions of E_T^{miss} and M_{T2}. As it is seen below there is an excellent agreement between Data and MC in both cases.

We also applied pile-up reweighting and b-tagging scale factor alongside of Jet-MET smearing and to see that these effects are under control and doing their jobs, we looked at the number of CSVT b jets, and it is clear that there is an excellent consistency between data and MC,

It was also checked the correlation of between variables M_{T2} and E_T^{miss} for different samples.

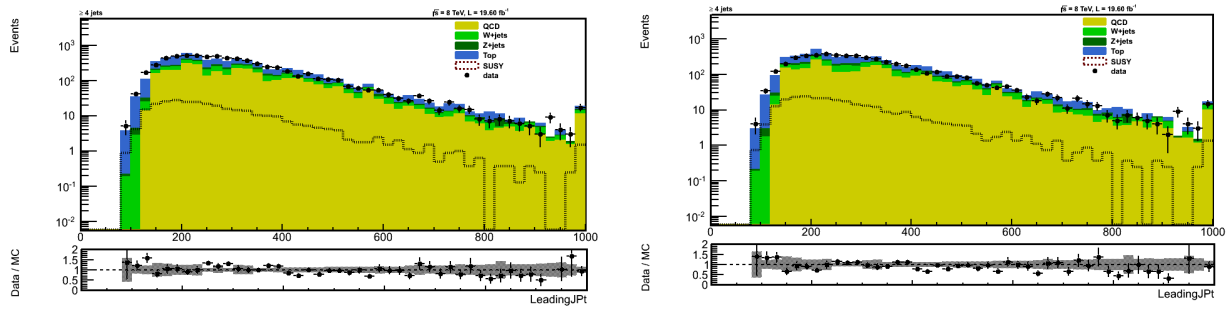

(a) (b)

Figure 12: Distribution of Leading Jet P_t before(a) and after(b) applying VSPT < 70

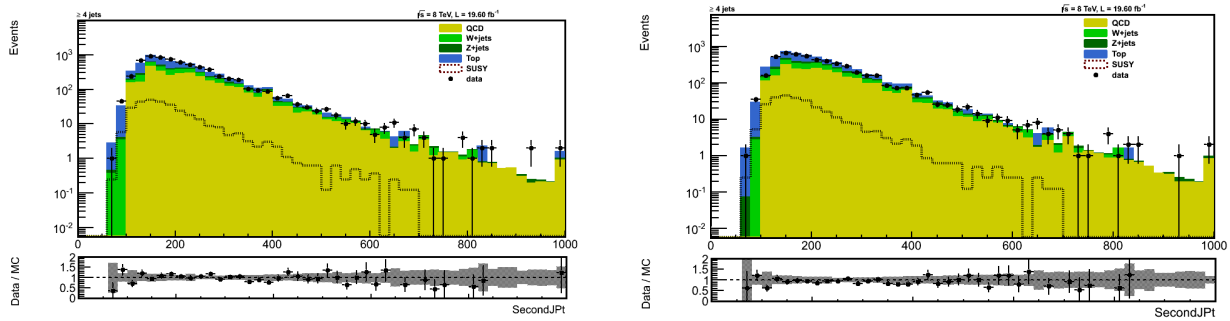

(a) (b)

Figure 13: Distribution of Second Jet P_t before(a) and after(b) applying VSPT < 70

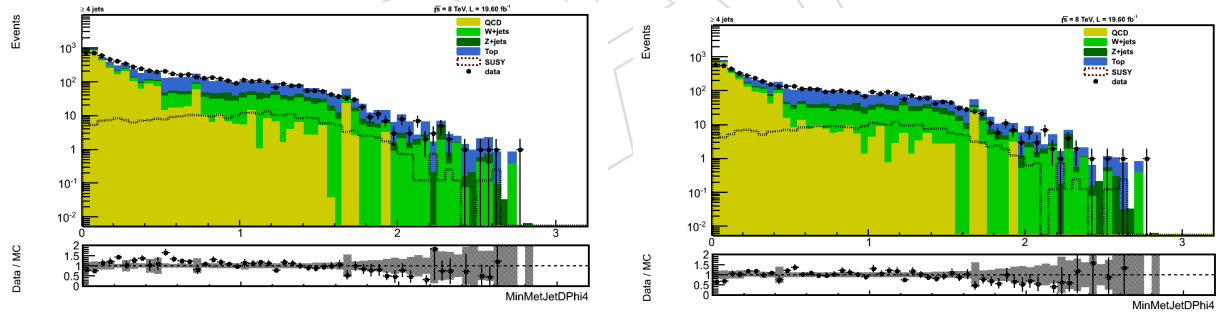

(a) (b)

Figure 14: Distribution of $\Delta\phi_4^{min}$ before(a) and after(b) applying VSPT < 70

It is seen that there is a correlation betwwn these two variables and events having hight E_T^{miss} sit in the high M_{T2} region.

To figure out the effects of pile-up reweighting, it was plotted the number of vertices before and after pile-up reweighting for data and MC samples which as it is seen below, this reweighting has no effecs on data but MC has been affected.

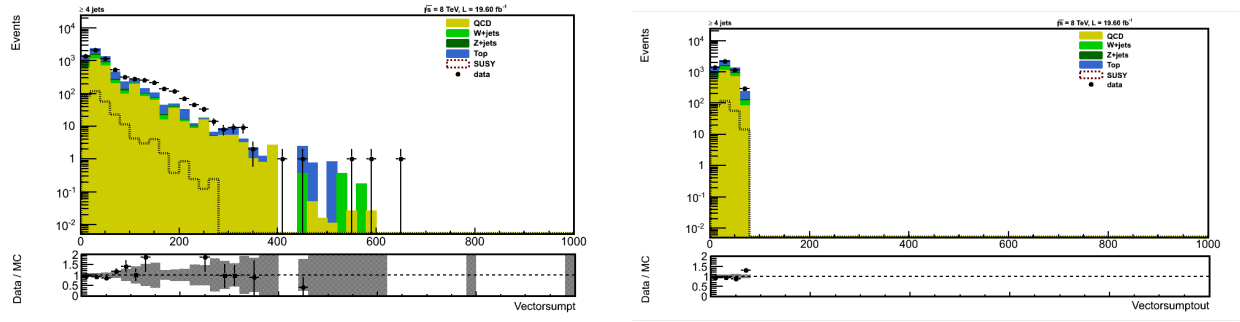

(a) (b)

Figure 15: Distribution of VSPT before(a) and after(b) applying VSPT < 70

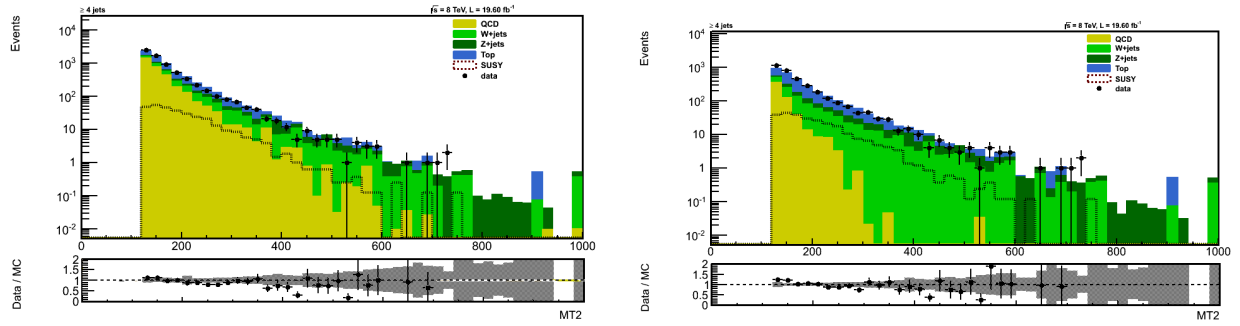

(a) (b)

Figure 16: Distribution of M_{T2} before(a) and after(b) applying $\Delta\phi_4^{min} > 0.3$

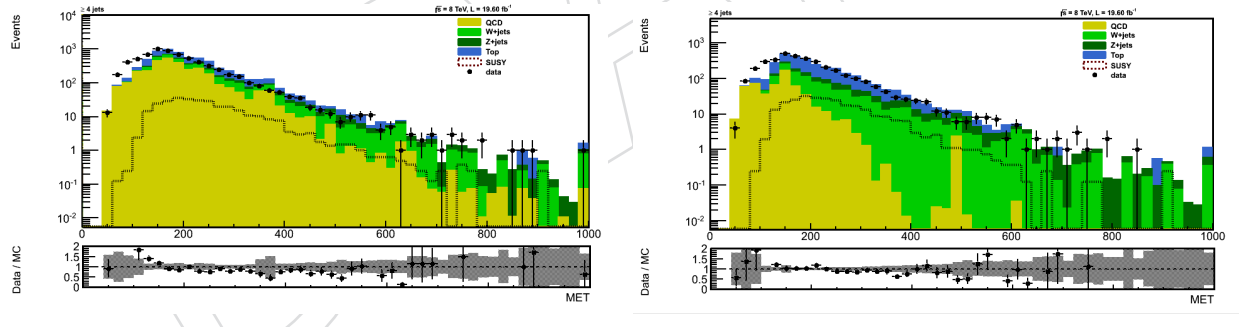

(a) (b)

Figure 17: Distribution of E_T^{miss} before(a) and after(b) applying $\Delta\phi_4^{min} > 0.3$

8 Search Strategy

The M_{T2} distribution in figure 28 is used as a variable to search for SUSY. With comparing the data and MC in the QCD dominated region ($M_{T2} < 60$ GeV), a flat scale factor of 1.19 is found for the QCD samples to have a good agreement between data and MC. To increase the power of the analysis, a multibinning approach is used. We select 4 bins in M_{T2} with the following edges 125, 150, 200, 250 and infinity. Every M_{T2} bin is devided to two bins with number of the reconstructed top quarks equal to 0 or greater than 0. There will be 8 bins in the analysis. In this round of analysis, we try to emphasize the complementary role of this anaysis for the common cut and count hadronic search for the direct stop production. Since this analysis, does

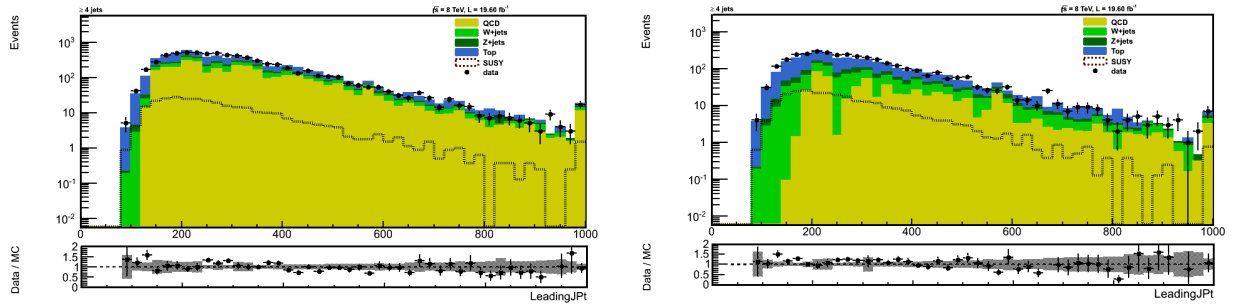

(a) (b)

Figure 18: Distribution of Leading Jet P_T before(a) and after(b) applying $\Delta\phi_4^{min} > 0.3$

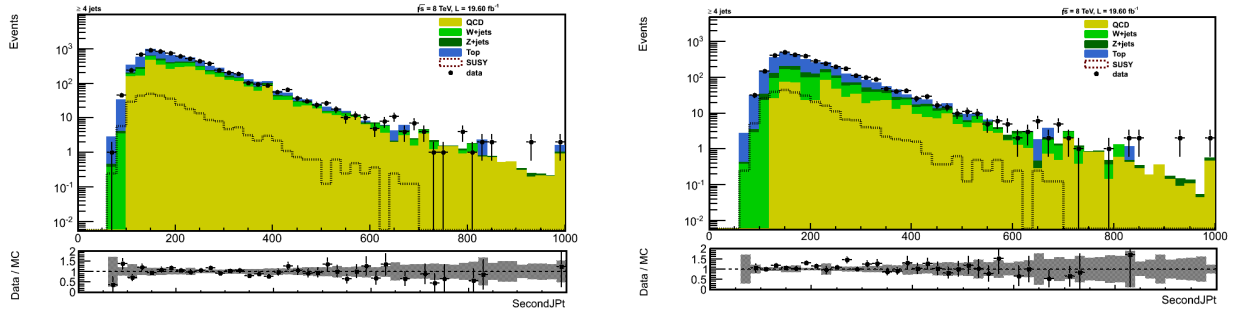

Figure 19: Distribution of Second Jet P_T before(a) and after(b) applying $\Delta\phi_4^{min} > 0.3$

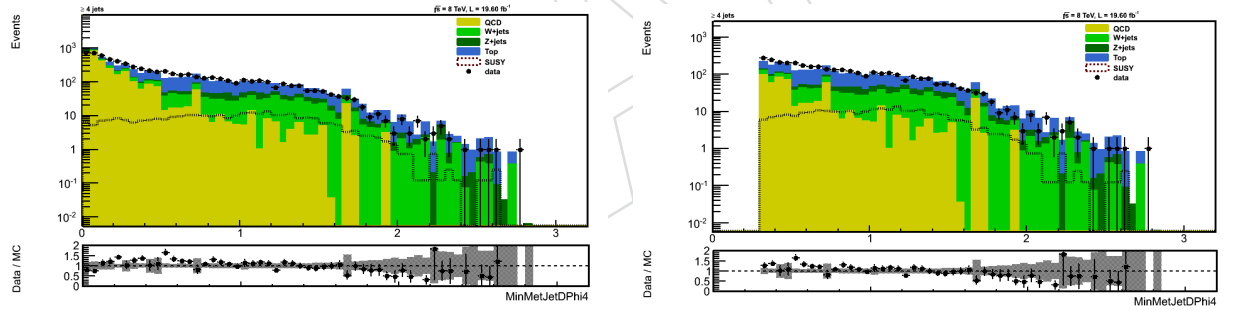

(a) (b)

Figure 20: Distribution of $\Delta\phi_4^{min}$ before(a) and after(b) applying $\Delta\phi_4^{min} > 0.3$

not use the MET explicitly, it is more sensetive to the small mass differences between stop and LSP.

9 Backgrounds

In this section, data driven methods are proposed and applied to estimate the contribution of the main background processes. Most of the methods are similar to what were used in the M_{T2} analysis [2] with some minor changes which are explained here.

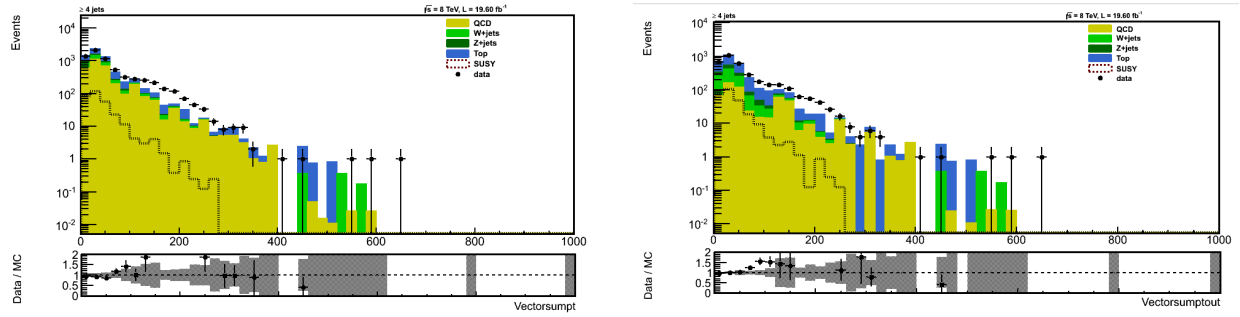

(a) (b)

Figure 21: Distribution of VSPT before(a) and after(b) applying $\Delta\phi_4^{min} > 0.3$

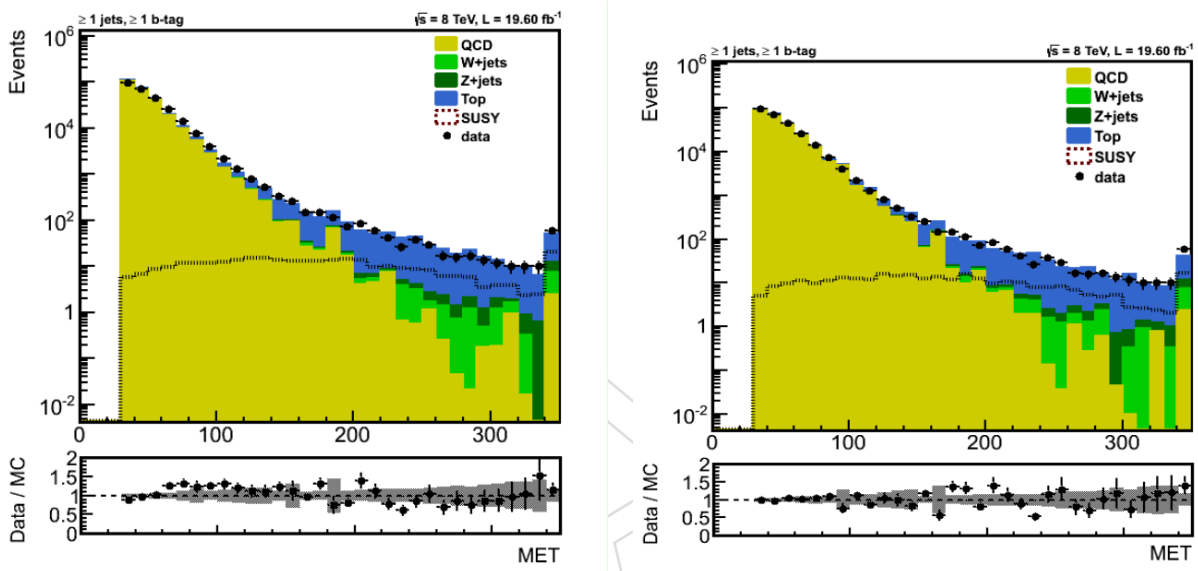

(a) (b)

Figure 22: Distribution of E_T^{miss} before(a) and after(b) applying Jet-MET smearing

9.1 Data-driven background estimation of QCD

Due to inadequate statistics of QCD Monte-Carlo samples and complicated nature of this background, we use a data driven method to estimate its rate in the tail of the M_{T2} distribution, while the simulation shows that it is negligible. f We follow the method, fully discussed and applied by the M_{T2} and M_{T2b} groups [2], but the parameters are finely tuned to the conditions of our analysis. The method indeed relies on different distributions of QCD and SUSY-like events in the plane of M_{T2} and $\Delta\phi_4^{min}$, the azimuth-difference between the E_T^{miss} vector and the closest selected jet.

Figure 29 shows such distributions for QCD (left) and SMS samples (right). Unlike the broad spread of SMS events in this plane, QCD events are densely populated in the low $\Delta\phi_4^{min}$ and M_{T2} region. Due to the strong correlation between the two variables of $\Delta\phi_4^{min}$ and M_{T2}, the usual ABCD method is inefficient, whereas a factorization method [2] is still applicable. The method works based on the ratio of $r(M_{T2}) = N(\Delta\phi_4^{min} \geq 0.3)/N(\Delta\phi_4^{min} \leq 0.2)$ as a function of M_{T2} for QCD events. Figure [30] shows the ratio $r(M_{T2})$ in the QCD simulation. It indicates an exponentially descending behavior in the region of $M_{T2} > 50$ GeV (the lower bins of M_{T2}

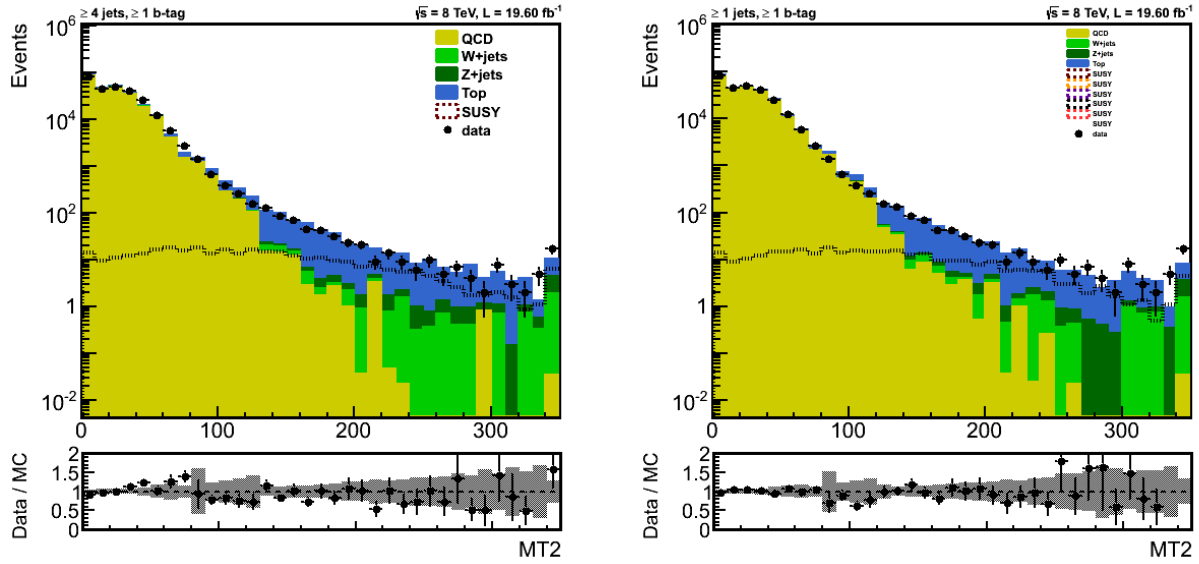

(a) (b)

Figure 23: Distribution of M_{T2} before(a) and after(b) applying Jet-MET smearing

could be biased by the minimal cut on E_T^{miss}). Hence, we characterize such specification of the QCD events by the model of

$$r(M_{T2}) = \frac{N(\Delta\phi_4^{min} \geq 0.3)}{N(\Delta\phi_4^{min} \leq 0.2)} = e^{a-b.M_{T2}} + c \tag{7}$$

where a and b parameters indicate respectively the slope and the intercept of the straight line in the logarithmic scale. Ratio $r(M_{T2})$ tends towards constant value, c, at large values of M_{T2}. The red curve in Figure 30 shows the fit of model (Equation 7) to the QCD simulation and Table 6 presents the value of parameters as a result of the fit in the range of $M_{T2} > 60$ GeV (the first column).

Parameter	$M_{T2} > 60$ GeV	$60 < M_{T2} < 80$ GeV
a	2.78 ± 0.17	2.94 ± 0.41
b (GeV^{-1})	0.0320 ± 0.0021	0.0325 ± 0.0058
c	0.0139 ± 0.0076	-

Table 6: The result of the two different parametrizations for ratio $r(M_{T2})$ in QCD simulated events.

In real data, to have a pure QCD sample with the minimal contamination from non-QCD backgrounds, we have to concentrate on the region of low M_{T2} ($60 < M_{T2} < 80$ GeV). The fit of ratio $r(M_{T2})$ on this short range of M_{T2} can be reasonably described as a straight line in the logarithmic scale. Thus, it is not able to give parameter c. The green curve in Figure 30 shows the linear fit and the second column of Table 6 presents the relevant parameters, a and b. As seen from Figure 30, both fits (green and red) are in a very good agreement at low M_{T2}, while the second fit (the green straight line), called optimistic parameterization, gives the lower values for ratio $r(M_{T2})$ at high M_{T2}. Hence, a realistic model needs also the parameter c to parameterize the ratio $r(M_{T2})$ in the entire range of M_{T2}. we conservatively take the parameter

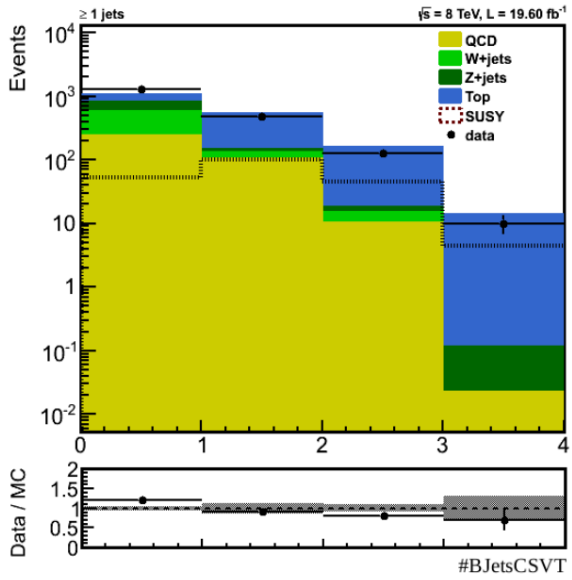

(a).no scale factor,no pile-up, no Jet-MET smearing

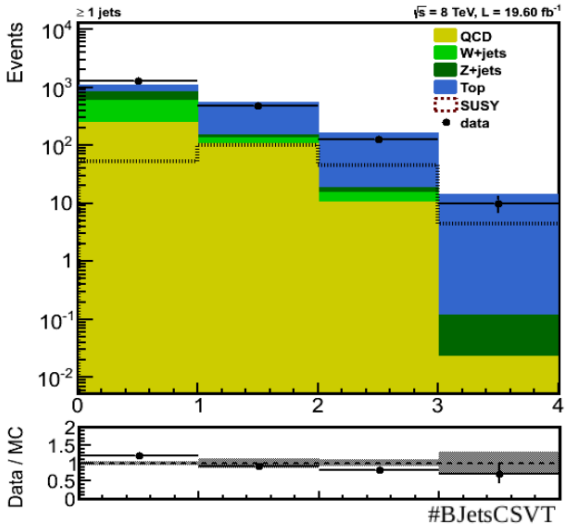

(b).no scale factor,no pile-up,Jet-MET smeared

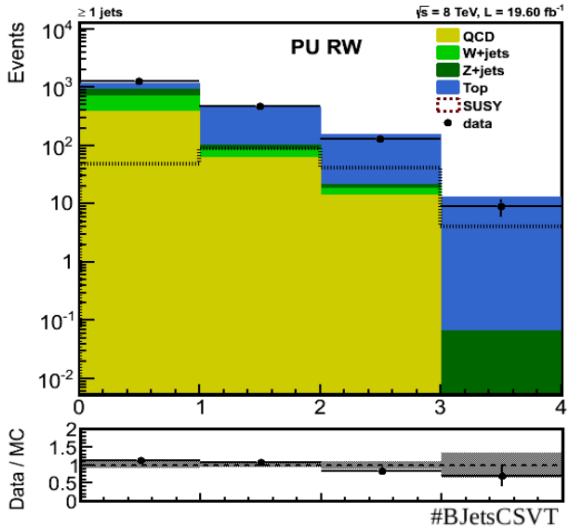

(c).no scale factor,pile-up reweighted,Jet-MET smeared

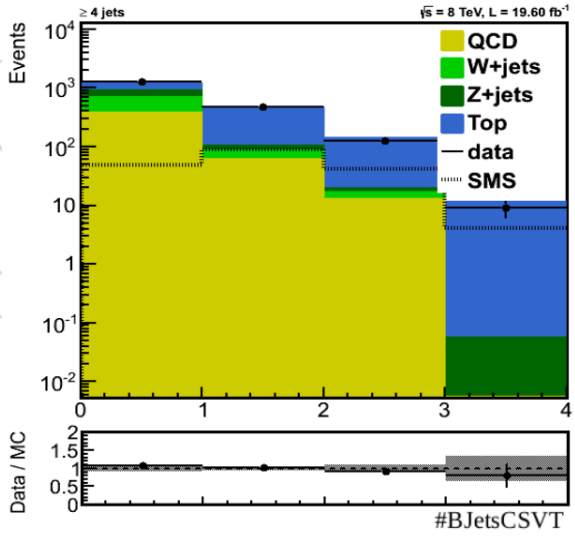

(d.scale factor applied ,pile-up reweighted,Jet-MET smeared)

Figure 24: Effects of applying Jet-MET smearing, pile-up reweighting and b-tagging scale factor on distribution of number of CSVT b jets

c from the straight line at $M_{T2} = 200$ GeV. The blue curve of Figure 30 represents such a fit, namely pessimistic parameterization.

Figure 31 depicts both parameterizations (optimistic and pessimistic by green and blue curves respectively) as a consequence of employing the method in the cleaned data. The non-QCD contaminations, taken from the Monte-Carlo simulation, are subtracted from data before calculating the parameters. Table 7 presents the parameters a and b extracted from the fit. These data-driven parameters eventually fulfill the functional form of ratio $r(M_{MT2})$.

In the last step of procedure, we apply the ratio $r(M_{T2})$ to the observed cleaned data in the QCD control region (high M_{T2}, low $\Delta\phi_4^{min}$) to estimate the number of QCD events in the signal

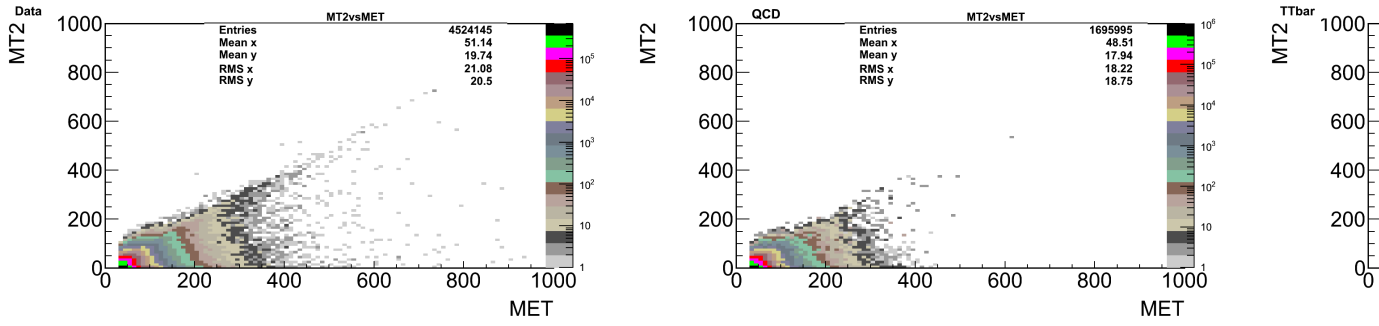

(a).data sample (b).QCD sample

Figure 25: Scatter plot of E_T^{miss} and M_{T2}

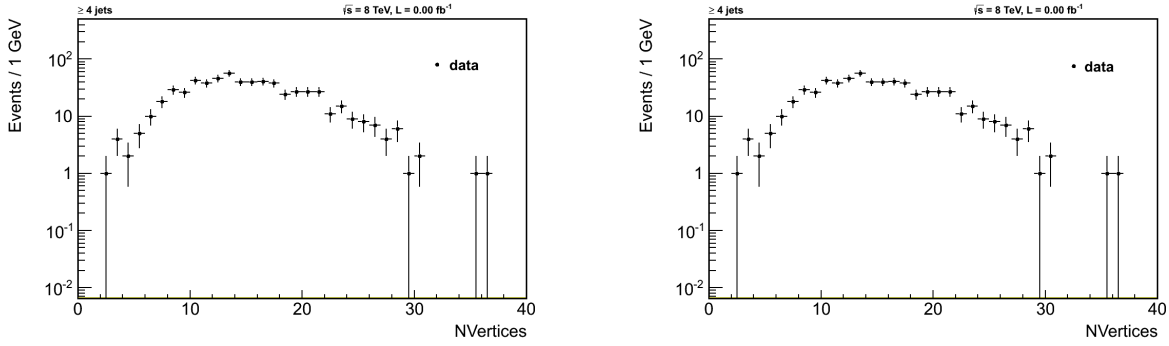

(a) (b)

Figure 26: Distribution of number of vertices for data before(a) and after(b) pile-up reweighting

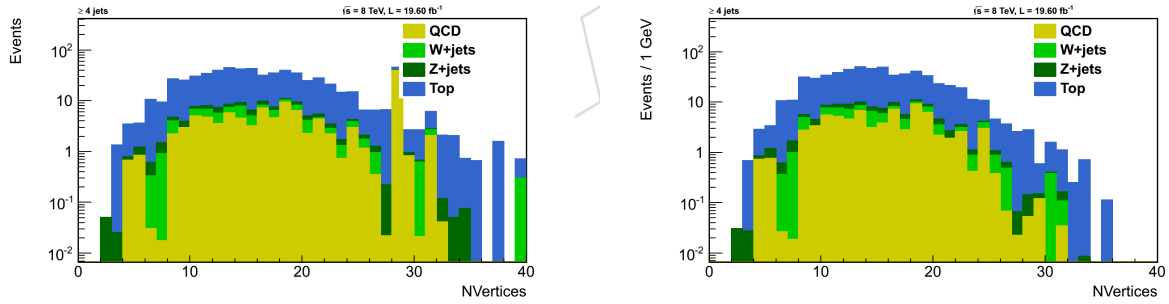

(a) (b)

Figure 27: Distribution of number of vertices for MC before(a) and after(b) pile-up reweighting

region (high M_{T2}, high $\Delta\phi_4^{min}$). Figure 32 shows the M_{T2} distribution of QCD truth observed events and the expected distribution from data (non-QCD subtracted). Furthermore, Table 8 compares the estimated with observed QCD events for several bins of M_{T2}. In addition to the statistical uncertainties, the predicted numbers incorporate the systematic ones, coming from the fit range. Indeed, the standard deviation of a 10% fluctuation at the boundaries of the fit range, $(60 < M_{T2} < 80)$ GeV, induces the systematic uncertainties reported in Table 8. Considering the uncertainties, the method prediction is in good agreement with the QCD truth.

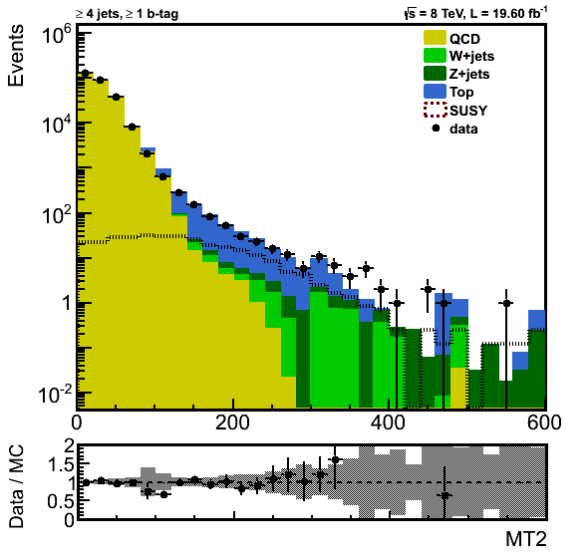

Figure 28: M_{T2} distribution after applying the full selection cuts.

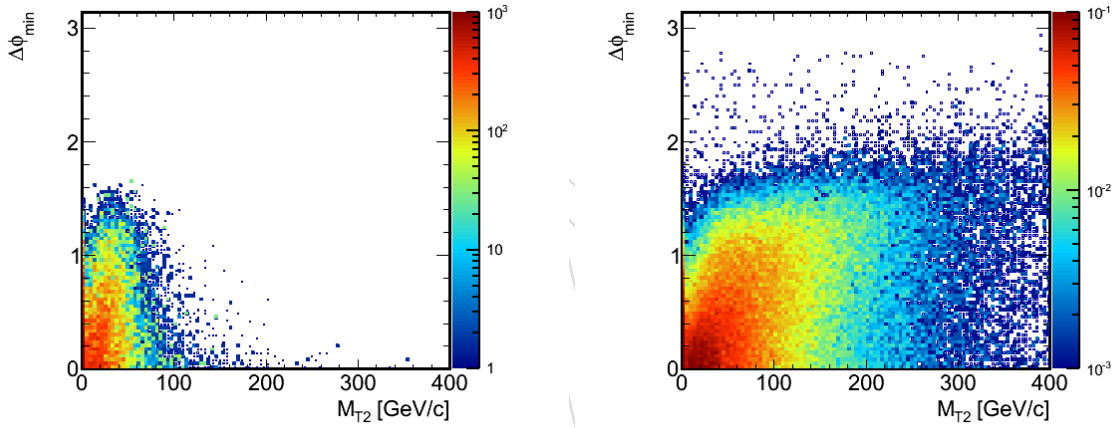

Figure 29: Distribution of $\Delta\phi_4^{min}$ versus M_{T2} for (left) QCD and (right) SUSY-like (SMS) simulated events. QCD events are populated in the low $\Delta\phi_4^{min}$ and M_{T2} region, while SUSY events spread over the plane.

9.2 Data-Driven Estimation of Lost Lepton from W+jets and Top

After applying the selection cuts, described in detail in Section 7, the background events are dominated by $t\bar{t}$ events. Among all decay channels of top pair system, it is mainly the semi-leptonic decay which contributes to the background. This can be understood because genuine neutrino is produced in the semi-leptonic decay of top pair system, $t\bar{t} \to W^+bW^-\bar{b} \to b\bar{b}l\nu_l jj$, which can pass the M_{T2} cut while the full-hadronic decay products, $t\bar{t} \to W^+bW^-\bar{b} \to b\bar{b}jjjj$, do not contain any neutrino. This section describes a method to estimate the backgrounds from the leptonic decay of W bosons, either from prompt production in W+jets events or from W bosons produced in single top and top pair events, shown as $t(\bar{t})$ for simplicity. The lepton is considered to be electron or muon.

Although the leptons are vetoed in the main analysis, but there are still some background from $W \to l\nu_l$, referred to as lost lepton background events, contributing to the full-hadronic analysis. This is due to the acceptance cuts or inefficiencies in the lepton isolation and identification criteria.

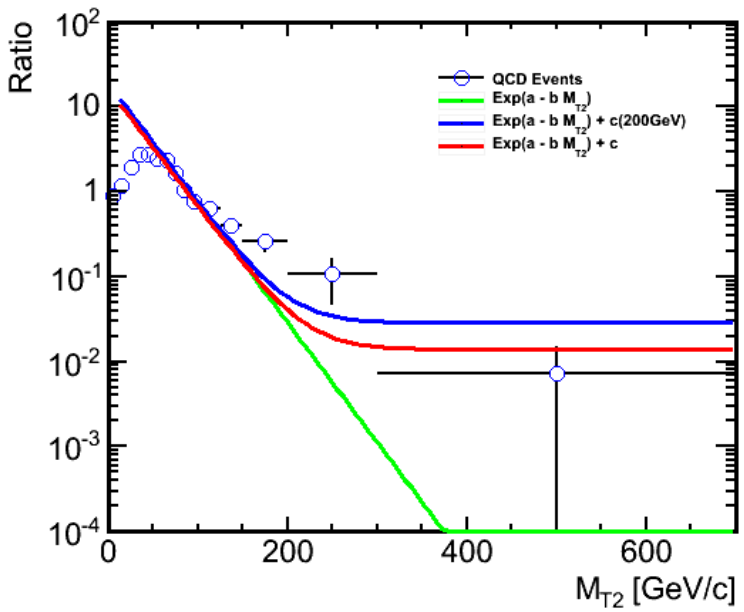

Figure 30: Three different fits of ratio $r(M_{T2})$ in QCD simulated events. The red curve is an exponential function plus a constant. It uses the entire range of $M_{T2} > 60$ GeV for parametrization (fully-MC) of ratio $r(M_{T2})$. The green curve is just an exponential function and uses the range of $60 < M_{T2} < 80$ GeV for parameterization (optimistic). The blue curve is also an exponential function plus a constant, however it uses the range of $60 < M_{T2} < 80$ GeV for parameterization (pessimistic).

Parameter	$60 < M_{T2} < 80$ GeV
a	2.41 ± 0.21
b (GeV^{-1})	0.0250 ± 0.0031

Table 7: The parametrization results for ratio r(M_{T2}) in real data (non-QCD events are subtracted, using simulation).

In order to estimate the backgrounds due to the lost lepton events, all selection cuts are applied except lepton veto which is inverted. The distribution of the p_T of the leptons in the events with exactly one lepton, being either electron or muon, are shown in Figure 33, where it can be seen that the number of MC events are greater than the observed number of data events.

In order to increase the data statistics, the cut on the $\Delta\phi_4^{min}$ is relaxed. While this cut was introduced in the main analysis to suppress the *QCD* background events, now that the lepton veto is reversed and exactly one lepton is required, the *QCD* events are still under control. Hence relaxing the $\Delta\phi_4^{min}$ cut would not be harmful. The only thing which should be taken into account is to consider the efficiency of this cut, called as f, which is explained in the following. The contribution of the lost lepton background events passing the lepton veto, shown as N_l^{pass}, is estimated with the following formula

$$\begin{aligned} N_l^{pass} &= (N_l^{reco} - N_l^{bg})\frac{1}{\varepsilon_l} - (N_l^{reco} - N_l^{bg}) \\ &= (N_l^{reco} - N_l^{bg})\frac{1-\varepsilon_l}{\varepsilon_l}, \end{aligned} \tag{8}$$

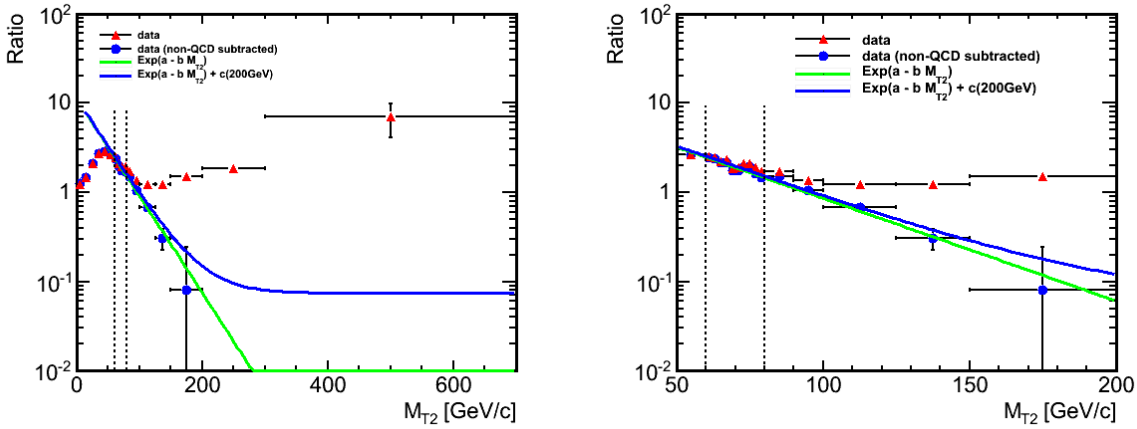

Figure 31: Fits of ratio $r(\ M_{T2})$ in the non-QCD subtracted data. The green and blue curves are related to optimistic and pessimistic parameterization respectively. The right plot is a focus on the desired range of M_{T2} for the parametrizations.

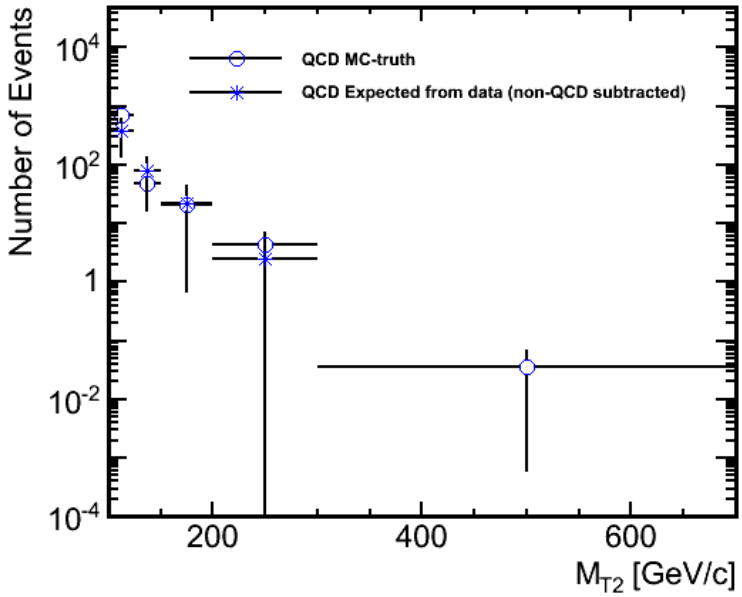

Figure 32: QCD MC-truth and data-driven prediction for the distribution of M_{T2}.

where N_l^{reco} refers to the number of data events with all selection cuts but the inverted lepton veto, which requires exactly one lepton. For this set of cuts, the number of background events from processes other than $W \to l\nu_l$ is represented by N_l^{bg} and is taken from MC. The ε_l contains the efficiency for a generated $W \to l\nu_l$ passing all selection cuts but the inverted lepton veto to have a lepton reconstructed. Here, the electron and muon efficiencies are obtained from both $t\bar{t}$ and $W + jets$ events and a relative contribution is used in the above formula. It should also be noted that, at the generator level, those $t\bar{t}$ events containing a tau lepton decaying hadronically are vetoed since these kind of events are considered when backgrounds from tau are estimated. In order to reduce the signal contamination in the leptonic signal region, a cut on the transverse

M_{T2} bins	MC-truth	Data-prediction
$[125, 150)$	48.1 ± 9.1	$78 \pm 62 \pm 95$
$[150, 200)$	20.7 ± 6.0	$22 \pm 22 \pm 60$
$[200, 300)$	4.5 ± 2.6	$2.4 \pm 3.1 \pm 15.2$
$[300, \infty)$	0.035 ± 0.034	$0.00 \pm 0.21 \pm 0.00$

Table 8: QCD MC-truth and data-driven prediction for the several bins of M_{T2}.

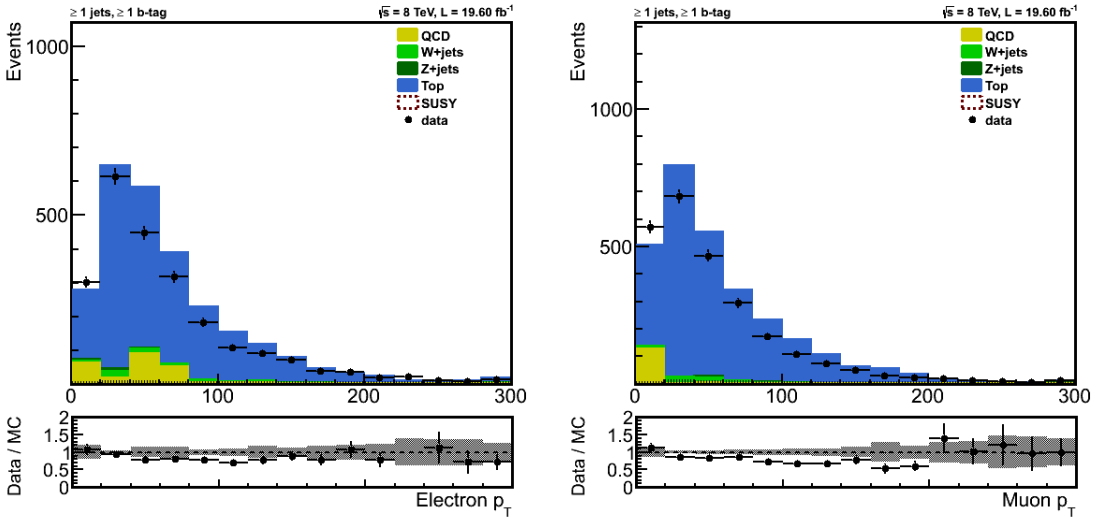

Figure 33: Left: The p_T distribution of the electrons in the events with one electron passing all selection cuts but the $\Delta\phi_4^{min}$ cut. The reason for this is stated in the text. No M_{T2} cut is applied in order to have more statistics. Right: The same plot for muons.

mass of the lepton, m_T, is applied which is defined as

$$m_T = \sqrt{2p_T(e,\mu)E_T^{miss}(1-\cos(\Delta\Phi))} < 100 \text{ GeV},$$

where $\Delta\Phi$ is the angle between lepton-p_T and E_T^{miss} in the transverse plane. In the $W \to l\nu_l$ events, the m_T cut represents the transverse mass of the W bosons which decreases above 80 GeV. Hence the leptonic signal events are not affected by this cut, while the contamination from SUSY events are strongly suppressed. The distribution of the m_T of either electrons or muons in the events with exactly one electron and one muon respectively, are shown in Figure 34. In this analysis, it is found that, e.g. for electron m_T distribution, the S/B decreases from 1.03% to 0.60% when $m_T < 100$ GeV cut is introduced. In the rest of this section, in addition to all selection cuts, the leptons are required to pass $m_T < 100$ GeV cut.

The fraction of events with all selection cuts with respect to the events with all selection cuts but the $\Delta\phi_4^{min}$ are shown in Figure 35 for data and MC. Since in the signal region, defined as region with $M_{T2} > 125$ GeV, the ratios become flat; therefore one can fit the ratios with a straight line. For both electrons and muons, the MC ratio is fitted and the fitted parameters f are quoted in Table 9.

The results of estimation of the lost lepton background events from data are summarized in Table 10. It should be mentioned that, the number of data events with one lepton selection and its corresponding background events are obtained from the relaxed cut selection, where $\Delta\phi_4^{min}$

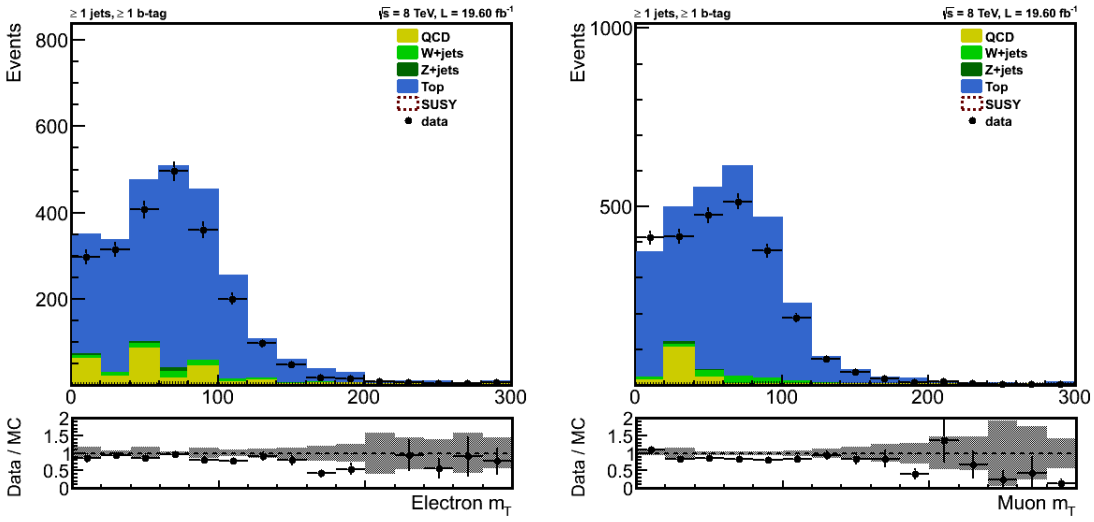

Figure 34: Left: The m_T distribution of the electrons for the events with one electron passing all selection cuts but the $\Delta\phi_4^{min}$ cut. The reason for this is stated in the text. No M_{T2} cut is applied in order to have more statistics. Right: The same plot for muons.

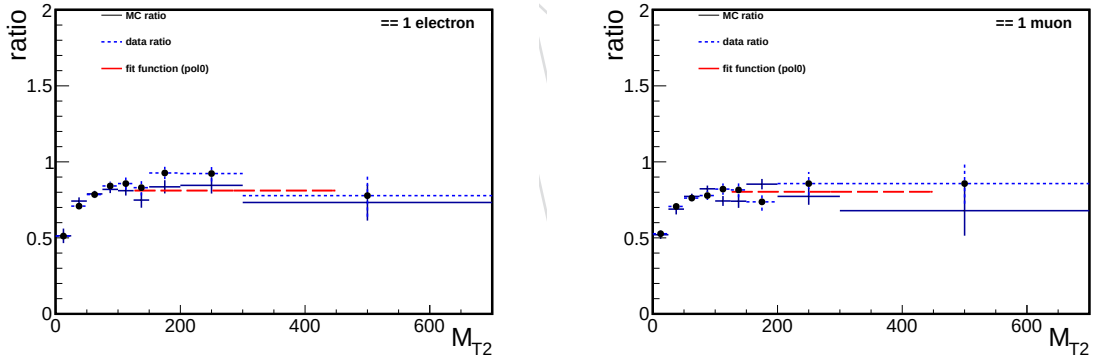

Figure 35: Left: Ratio between events with one electron passing all selection cuts versus events with one electron passing all selection cuts but the $\Delta\phi_4^{min}$ for data (blue) and MC (black). The fit line for the MC ratio over all M_{T2} signal bins is drawn in red. Right: The same plot for events with one muon.

	electrons	muons
Fit value for the ratio f	0.811 ± 0.028	0.804 ± 0.024

Table 9: Fit values f obtained from the MC ratios for electrons and muons.

is dropped. Therefore the prediction is corrected back by multiplying the event yield with the fitted ratio value f.

	N^{reco}	N^{bg}	R_{LL}	N^{pass} MC-Truth	N^{pass} data-prediction
electrons					
	129	20.78	1.18 ± 0.20	148.99 ± 9.66	$127.82 \pm 13.41(stat) \pm 32.41(sys)$
muons					
	150	26.04	0.66 ± 0.14	105.23 ± 8.14	$81.90 \pm 8.09(stat) \pm 24.29(sys)$

Table 10: Data-Driven Estimation of Lost Lepton from W+jets and $t(\bar{t})$ for electrons and muons. The lost lepton ratio R_{LL} is given by $f\frac{1-\varepsilon_l}{\varepsilon_l}$.

It should be noted that for the systematic uncertainty, two possible sources are taken into account. A first one is a systematic uncertainty of 100% on the number of backgrounds. A second one is a systematic uncertainty of 5%, considered when calculating the efficiencies ε_l from MC, to account for possible difference between data and simulation.

9.3 Estimation of the Tau Leptons

Tau leptons can decay hadronically and appear as a thin jet and enter the hadronic searches. To estimate the contamination from such events a method similar to what is used for the lost lepton background is used here. The number of events with exactly one real tau is corrected by accounting for the reconstruction and acceptance efficiencies. In the other words:

$$N_{W\to\tau\nu} = \frac{N_\tau^{reco} - N_\tau^{bg}}{\varepsilon_\tau}, \tag{9}$$

where N_τ^{reco} is the number of events with one reconstructed tau, N_τ^{bg} is the number of events with a fake tau and ε_τ denotes the probability for a generated $W \to \tau\nu$, $\tau \to had$ event passing the selection cuts to have a reconstructed and identified tau. The efficiency ε_τ is extracted from simulation. In average, ε_τ is found to be $\sim$ 24%. 5% systematic uncertainty is assigned to this value to take into account the differences between data and MC. The transverse mass (m_T) of the system of the reconstructed tau and MET is forced to be less than 100 GeV/c^2 to decrease the signal contamination. The number of events with a fake tau, N_τ^{bg} is found from the MC simulation and a 50% systematic uncertainty is assigned to this value.

The M_{T2} distribution of the events with all selection cuts which have an identified tau in the final state is shown in Figure 36. Scale factors of the tau selection are not applied and it can be the source of the discrepancies between data and MC. In Table 11 contribution of different

M_{T2} (GeV)	QCD	Z+Jets	W+Jets	Top	MC(sum)	data
full range	4544.26	8.68	27.99	1074.53	5655.47 ± 794.11	6226.00
$125 - \infty$	0.00	0.19	5.74	58.98	64.91 ± 6.69	61.00
cut on $\Delta\phi_4^{min}$ is relaxed						
$125 - \infty$	5.83	0.19	10.06	81.38	97.46 ± 8.57	86.00

Table 11: MC and data event yields in full range and signal region. The last row shows the yields after relaxing the cut. The error on the total background is purely statistical.

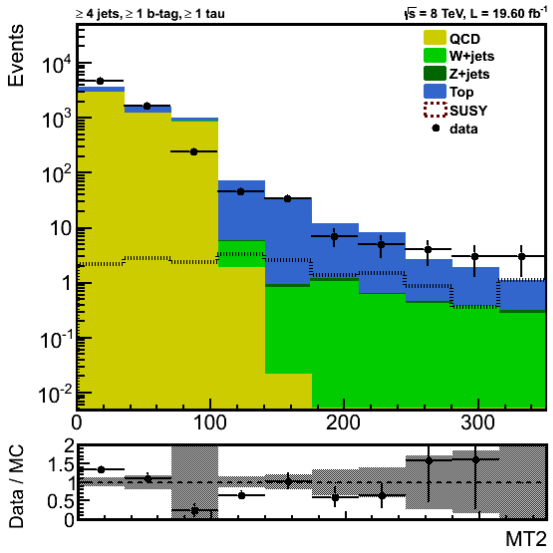

Figure 36: M_{T2} distribution for events with at least one tau in data and MC with all selection cuts.

samples in the plot of Figure 36 is shown. It can be seen that the statistics in the signal region is poor. To decrease the uncertainties of the predictions, the cut on $\Delta\phi_4^{min}$ is relaxed. The last row of the table shows the statistics after this relaxation. The scale factor to compensate this relaxation is read from MC.

Table 12 shows the performance of the method on MC and data. The quoted uncertainties of

M_{T2} bin	MC Truth	Prediction in MC	Prediction in Data
$125 - \infty$	230.56 ± 14.82	$237.45 \pm 26.62 \pm 35.81$	$201.82 \pm 28.82 \pm 31.39$

Table 12: Prediction of the tau contamination in the signal region in both data and MC.

the predictions are statistical and systematical, respectively.

9.4 Estimation of Invisible Z Background from Data Using W +jets Events

To estimate $Z \to \nu\bar{\nu}$ background we use $W \to \mu\nu$+jets events. The kinematics of leptons as well as the jets are very similar in both Z+jets and W+jets processes. Besides, the larger cross-section of W+jets allows for a more precise estimation of $Z \to \nu\bar{\nu}$. This is a well studied method in various analyses within the CMS Collaboration (see e.g. [14–16]). To make the event kinematics compatible from the E_T^{miss} point of view, the p_T of muon is added to the one of neutrino in W+jets events. The M_{T2} variable and other quantities related to E_T^{miss} are recalculated accordingly. This estimation can be described as:

$$N_{Z\to\nu\bar{\nu}}(est) = N_{W(\mu\nu)} R^{MC} \frac{1}{\epsilon_{acc}\epsilon_{reco/iso}}. \quad (10)$$

where,

- ϵ_{acc} is the muon acceptance derived from MC.
- $\epsilon_{reco/iso}$ is the muon reconstruction and isolation efficiency, taken from data using the Tag&Probe method.
- R^{MC} corrects kinematic, selection and cross-sections differences between $Z \to \nu\bar{\nu}$ and $W \to$

$\mu\nu$+jets processes.

- $N_{W(\mu\nu)}$ is the number of selected $W \to \mu\nu$+jets events.

The selection is similar to the one of signal where the lepton veto is reduced to an electron veto. In addition we request for the presence of exactly one reconstructed muon passing all the quality and isolation cuts, with $p_T > 10$ GeV and $|\eta| < 2.4$. The W-boson transverse mass (using default E_T^{miss}) is required to be $m_T < 100$ GeV in order to reduce other backgrounds and signal contaminations. To enrich the sample with W+jets and to reject $t\bar{t}$ events, we veto events with at least one b-tagged jet where the medium working point of CSV b-tagging algorithm is applied on jets with $p_T > 20$ and $|\eta| < 2.4$. The results of this selection for MC samples and data are summarized in Table 13. The distributions of muon p_T, M_{T2} and m_T for this region are shown in Figures 37a, 37b and 37c and as it is seen there is a good agreement between data and MC in W enriched region.

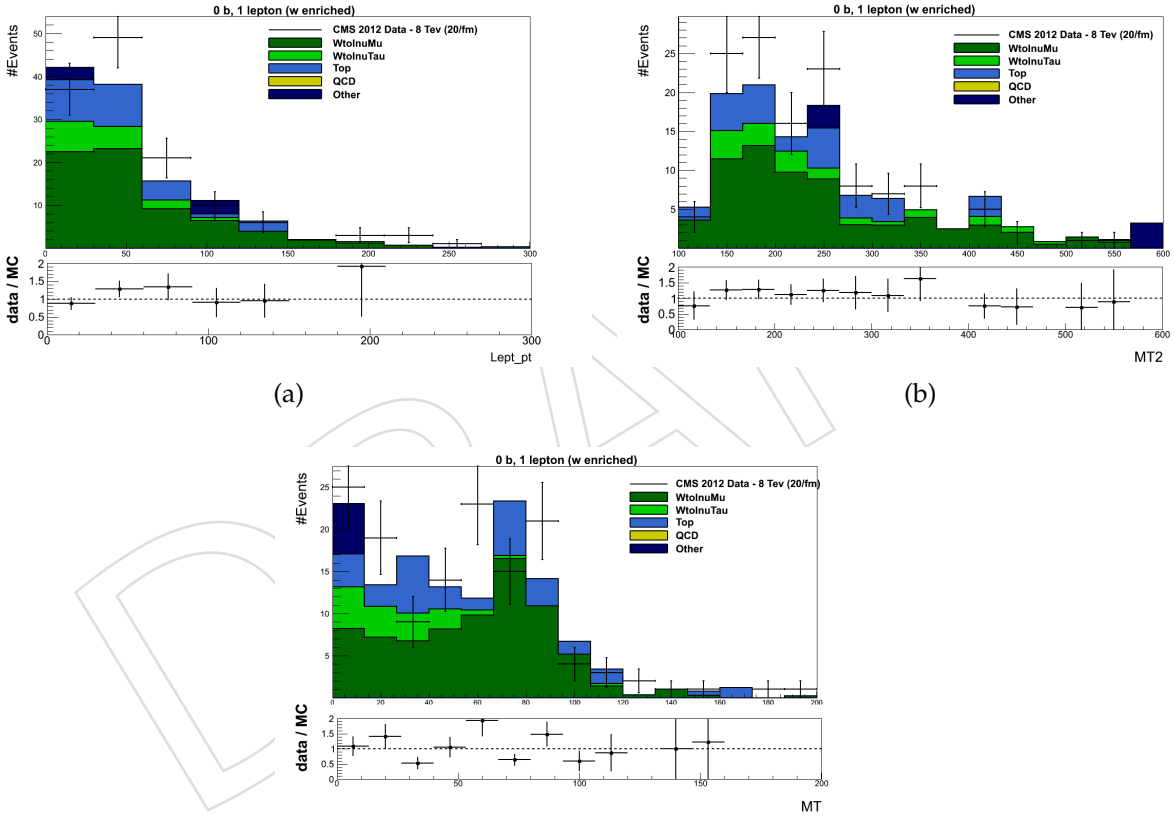

(a) (b)

(c)

Figure 37: Muon p_T, M_{T2} and m_T distributions for W-enriched region

9.4.1 $t\bar{t}$ background estimation in W-enriched sample

Despite of b-tag veto some top events remain in W enriched region. The contribution of $t\bar{t}$ is estimated from data while for the rest of backgrounds we trust on simulation. The b-tag veto is relaxed and at least one b-jet is requested to obtain a sample enriched in top events. The selection results are shown in Table 14. To find out the number top events in b-tag veto region

	WtolnuMu	WtolnuTau	QCD	Zinv	Top	SMS	Other	MC	data
All events (jets $\geq$ X)	145.81	230.75	462.23	235.41	1314.11	0.00	184.86	2573.17 +- 80.53	2510.00
Analysis selection cuts	145.81	230.75	462.23	235.41	1314.11	0.00	184.86	2573.17 +- 80.53	2510.00
Lepton Veto	145.81	214.43	459.75	235.29	1068.30	0.00	96.65	2220.23 +- 78.92	2192.00
Lepton Selection	91.76	17.61	0.74	0.11	277.43	0.00	6.00	393.65 +- 16.96	329.00
$m_T < 100\,\text{GeV}$	83.26	17.30	0.74	0.06	241.95	0.00	6.00	349.30 +- 15.99	293.00
b-jets Selection	69.67	15.29	0.00	0.03	27.85	0.00	6.00	118.83 +- 8.25	130.00
M_{T2} 100 - 150 GeV	8.97	1.56	0.00	0.00	4.67	0.00	0.00	15.20 +- 2.69	12.00
M_{T2} 150 - 200 GeV	19.28	4.94	0.00	0.03	6.61	0.00	0.00	30.86 +- 3.67	44.00
M_{T2} 200 - 275 GeV	19.45	4.09	0.00	0.00	8.71	0.00	2.88	35.14 +- 4.75	41.00
M_{T2} 275 - 375 GeV	9.80	2.25	0.00	0.00	4.19	0.00	0.00	16.24 +- 2.71	21.00
M_{T2} 375 - 500 GeV	7.39	2.08	0.00	0.00	2.57	0.00	0.00	12.04 +- 2.33	7.00
$M_{T2} > 500$ GeV	4.08	0.37	0.00	0.00	1.10	0.00	3.12	8.67 +- 3.43	5.00

Table 13: Yields for the W-enriched selection

(W enriched), b-tagging (in)efficiency has to be considered. This process can be described as:

$$N_{top}(b-veto) = N_{top}(\geq 1b-tag)\frac{\epsilon(b-veto)}{\epsilon(\geq 1b-tag)}, \tag{11}$$

where the $\epsilon(b-veto)$ and $\epsilon(\geq 1b-tag)$ are the efficiencies of vetoing or selecting b-tagged events and are taken from simulation, thus corrected by the data-simulation scale factors given by the b-tag POG for the CSVE (0.963 ± 0.020) and CSVT(0.947 ± 0.025) working points, respectively [17]. As it is apparent from Table 14 there is a good agreement between data and MC in top-enriched region and also the Muon p_T, M_{T2} and m_T distributions are shown in Figures 38a, 38b and 38c, respectively.

	WtolnuMu	WtolnuTau	QCD	Zinv	Top	SMS	Other	MC	data
All events (jets $\geq$ X)	170.32	267.04	493.27	270.57	1122.03	0.00	211.59	2534.83 +- 86.48	2510.00
Analysis selection cuts	170.32	267.04	493.27	270.57	1122.03	0.00	211.59	2534.83 +- 86.48	2510.00
Lepton Veto	170.32	248.45	490.77	270.43	913.06	0.00	109.45	2202.48 +- 85.20	2192.00
Lepton Selection	107.15	20.76	0.62	0.12	236.72	0.00	5.85	371.23 +- 15.38	329.00
$m_T < 100\,\text{GeV}$	97.37	20.36	0.62	0.06	206.08	0.00	5.85	330.34 +- 14.53	293.00
b-jets Selection	5.71	1.06	0.61	0.00	141.35	0.00	0.00	148.74 +- 10.24	119.00
M_{T2} 100 - 150 GeV	0.64	0.41	0.00	0.00	16.11	0.00	0.00	17.16 +- 3.47	28.00
M_{T2} 150 - 200 GeV	0.31	0.34	0.61	0.00	53.26	0.00	0.00	54.53 +- 6.38	43.00
M_{T2} 200 - 275 GeV	1.46	0.00	0.00	0.00	43.72	0.00	0.00	45.18 +- 5.64	26.00
M_{T2} 275 - 375 GeV	1.94	0.00	0.00	0.00	24.37	0.00	0.00	26.30 +- 4.14	16.00
M_{T2} 375 - 500 GeV	0.68	0.00	0.00	0.00	1.79	0.00	0.00	2.47 +- 1.17	3.00
$M_{T2} > 500GeV$	0.69	0.30	0.00	0.00	1.30	0.00	0.00	2.29 +- 1.10	2.00

Table 14: Yields for the top-enriched selection

9.4.2 Z Estimation Results

After finding the number of top events in the b-tag veto (W-enriched) region, it is subtracted from the number of W's of this region, derived from data, to obtain the correct number of $W \to \mu\nu$ events. Due to requesting one b-jet in the final state we need to have the number of W's in 1 b-tag region to be able to estimate the number of Z in this region. Therefore we must multiply the number of W's in b-tag veto region to $\frac{\epsilon(1bW)}{\epsilon(0bW)}$ to reach the number of W's in 1 b-tag region and this ratio is coming from MC and it is considered b-tag scale factor.

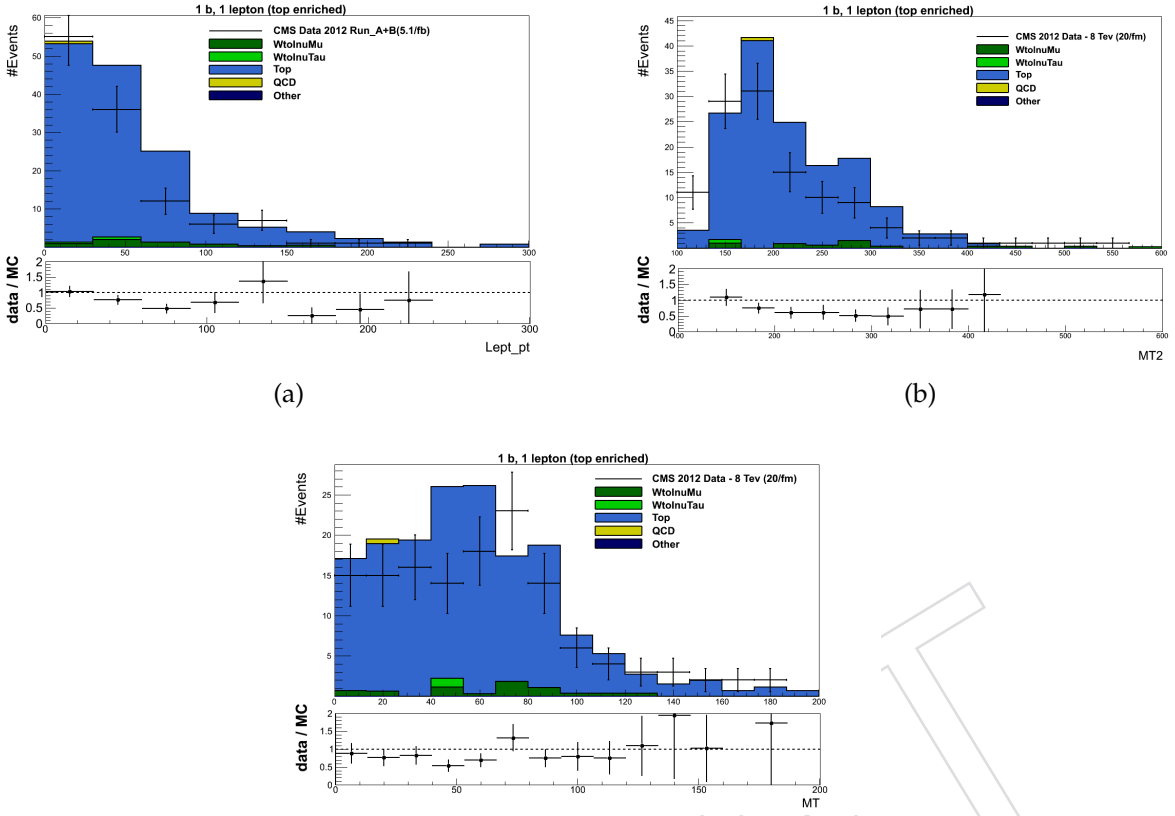

(a) (b)

(c)

Figure 38: Muon p_T, M_{T2} and m_T distributions for top-enriched region

9.4.3 Systematic uncertainties

The systematic uncertainty on $Z \to \nu\nu$ estimation has contributions from different sources, as can be seen in Equation 10. There, the uncertainty on R^{MC} is taken from simulation where it includes the uncertainties due to the PDF set and the k-factor [FIXME?] in Z and W bosons production rates. The uncertaintiy on the muon acceptance efficiency is derived from simulation, too. The muon selection efficiency ($\epsilon_{reco/iso}$) as well as its uncertainty are data-driven, obtained from the Tag&Probe method. Another uncertainty in this estimation arises from the requirement of $m_T < 100\,\text{GeV}$ which is estimated from simulation.
For the $N_{W(\mu\nu)}$ in the analysis region with at least one b-tagged jet, the $N_{W(\mu\nu)}$ estimation in b-tag veto region is corrected with the data-driven b-tagging and b-tag veto efficiencies. The uncertainties on these efficiencies are taken from data, accordingly.
Other than $t\bar{t}$, all backgrounds and their uncertainties are estimated from simulation in $N_{W(\mu\nu)}$ calculation. The $t\bar{t}$ contribution in W-enriched (b-tag veto) region is obtained using Equation 11. In this estimation, the uncertainties on b-tagging efficiencies are taken from data while the background uncertanties are derived from simulation.

The final estimation together with their uncertainties are summarized in Table 15.

	MC	Data Estimation
top (0b, 1l)	27.85 ± 4.68	18.73 ± 4.56 (1.72 (stat) $\pm$4.22 (syst))
W (0b, 1l)	69.67 ± 4.79	89.98 ± 13.71 (8.08 (stat) $\pm$ 11.08 (syst))
Zinv (1b, 0l)	22.74 ± 0.84	19.68 ± 8.09 (1.77 (stat) $\pm$7.89 (syst))

Table 15: Z-invisible Estimation

10 Statistical Interpretation of the results

Since no excess of data over the background prediction has been observed, we close our study with setting upper limits on the testing signals. This is conducted using a modified frequentist approach, namely CLs method [18]. In this method, the test statistic q_μ [19] is a function of the profile likelihood-ratio,

$$q_\mu = -2 \ln \frac{\mathcal{L}(data;\, b + \mu s)}{\mathcal{L}(data;\, b + \hat{\mu} s)}, \tag{12}$$

where $\hat{\mu}$ is the *signal strength modifier* μ at the maximum point of the likelihood $\mathcal{L}$. Then CLs is given by the following probability-ratio,

$$CL_s = \frac{p(q_\mu \geq q_\mu^{obs} | b + \mu s)}{p(q_\mu \geq q_\mu^{obs} | b)}. \tag{13}$$

We compute CLs using a software package provided by the CMS Higgs PAG [20]. After incorporating systematic uncertainties, an observed CLs smaller than 0.05 for a signal strength of $\mu = 1$, excludes the given signal at 95% CL. Indeed, the package determines which signal strength μ excludes the testing signal at 95% CL. Therefore all resulting $\mu \leq 1$ define the excluded region in the parameter space of the given signal.

In this study, we analyze data in 8 different bins (multi-bin analysis) to utilize more information from the observed and the predicted distributions. The bins are defined in reconstructed top quark multiplicity, zero or more. In addition, events are categorized based on the M_{T2} values: 125GeV $\leq$ M_{T2} $<$ 150GeV, 150GeV $\leq$ M_{T2} $<$ 200GeV, 200GeV $\leq$ M_{T2} $<$ 250GeV, 250GeV $\leq$ M_{T2} $< \infty$.

To investigate the exclusion power of our research, we study the topology of direct stop pair production in Simplified Models [21], with $\tilde{t} \rightarrow \tilde{\chi}_1^0 t$ (T2tt). The research excludes a sizable region of the phase space, surrounded by the lines of $m_{\tilde{t}} = 600$GeV and $m_{LSP} = 175$GeV with an integrated luminosity of 19.6 fb^{-1}.

Figure 39 shows the expected upper limit on the cross section of the stop pair production in terms of Simplified Models. Furthermore, the figure shows the expected exclusion power considering 40% systematic uncertainties on signal and background rates which are predicted using Monte-Carlo simulations. The black dashed curve represents the expected reach by the common Cut&Count [22] search using E_T^{miss} trigger. As the figure shows our analysis (the blue solid curve) can be comparable with other analyses and it has the potential to be complementary to other analyses in some regions of the phase space.

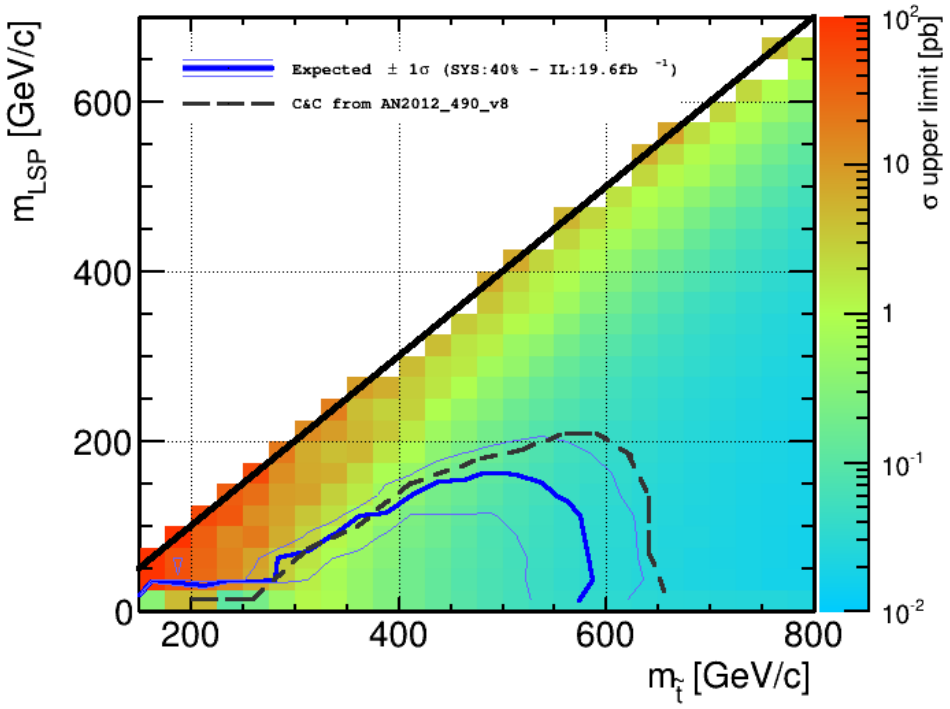

Figure 39: Expected exclusion power in terms of Simplified Models (T2tt-topology) with an integrated luminosity of 20 fb^{-1}. Backgrounds are predicted using Monte-Carlo simulations and a rough estimate of systematic uncertainties equal 40% is taken into account.

11 Conclusion

A hadronic search for direct Stop production is presented using the M_{T2} variable. Data driven methods are used to estimate the main backgrounds. It is shown that the methods close properly on MC. Since the analysis uses a multijet trigger and M_{T2} does not depend explicitly on E_T^{miss}, it can be complementary to the common cut and count search for Stop which uses E_T^{miss} trigger. It is shown that in the regions with low mass difference between $m_{\tilde{t}}$ and m_{LSP} this analysis can have a comparable reach.

12 Outlook of the Analysis

In the next step, the set of data known as "Parked data" will be used. Thanks to the looser triggers in the "Parked data", it is expected to have a better signal efficiency when the analysis applied on this data. Re-optimizing the analysis with these looser triggers is foreseen for next steps to improve the reach even further.

13 Acknowledgements

This analysis benefits highly from the computing resources and codes developed in ETHZurich. We appreciate their help and generosity. The method used for the top reconstruction was firstly introduced and implemented by L. Pape. We thank him for providing us the code and giving useful comments in some parts of the analysis. The authors would like to thank the conveners of the SUSY-TBT working group, Rick Cavanaugh and Juan

Alcaraz Maestre, for their help and support. Batool Safarzadeh has read the analysis and provided some useful comments, we appreciate her help. The authors would like to thank the management and staff of the school of particles and accelerators of IPM, especially Prof. Arfaei for their help and support. Thanks to all of the members of the CMS collaboration for their outstanding results discussed partly here.

References

[1] S. P. Martin, "A Supersymmetry primer", arXiv:hep-ph/9709356.

[2] Casal et al., "Search for supersymmetry in hadronic final states using MT2 based on 4.4/fb of CMS data at sqrt(s) = 7 TeV", CMS Analysis Note 2012/040, CERN, (2012).

[3] H. Bakhshian et al., "A Hadronic Search for Direct Stop with MT2 Variable", CMS Analysis Note 2013/140, CERN, (2013).

[4] UA1 Collaboration Collaboration, "Experimental Observation of Isolated Large Transverse Energy Electrons with Associated Missing Energy at s**(1/2) = 540-GeV", *Phys.Lett.* **B122** (1983) 103–116, doi:10.1016/0370-2693(83)91177-2.

[5] UA2 Collaboration Collaboration, "Observation of Single Isolated Electrons of High Transverse Momentum in Events with Missing Transverse Energy at the CERN anti-p p Collider", *Phys.Lett.* **B122** (1983) 476–485, doi:10.1016/0370-2693(83)91605-2.

[6] CDF Collaboration Collaboration, "Measurement of the W boson mass with the Collider Detector at Fermilab", *Phys.Rev.* **D64** (2001) 052001, doi:10.1103/PhysRevD.64.052001, arXiv:hep-ex/0007044.

[7] D0 Collaboration Collaboration, "Improved W boson mass measurement with the DØ detector", *Phys.Rev.* **D66** (2002) 012001, doi:10.1103/PhysRevD.66.012001, arXiv:hep-ex/0204014.

[8] C. Lester and D. Summers, "Measuring masses of semiinvisibly decaying particles pair produced at hadron colliders", *Phys.Lett.* **B463** (1999) 99–103, doi:10.1016/S0370-2693(99)00945-4, arXiv:hep-ph/9906349.

[9] A. Barr, C. Lester, and P. Stephens, "m(T2): The Truth behind the glamour", *J.Phys.* **G29** (2003) 2343–2363, doi:10.1088/0954-3899/29/10/304, arXiv:hep-ph/0304226.

[10] W. S. Cho, K. Choi, Y. G. Kim, and C. B. Park, "Measuring superparticle masses at hadron collider using the transverse mass kink", *JHEP* **0802** (2008) 035, doi:10.1088/1126-6708/2008/02/035, arXiv:0711.4526.

[11] CMS Collaboration, "Search for Supersymmetry in hadronic final states using M_{T2} with the CMS detector at $\sqrt{s}$ = 7 TeV", CMS Physics Analysis Summary CMS-PAS-SUS-12-002, CERN, (2012).

[12] T. Sjöstrand, S. Mrenna, and P. Skands, "PYTHIA 6.4 physics and manual", *JHEP* **05** (2006) 026, doi:10.1088/1126-6708/2006/05/026, arXiv:hep-ph/0603175.

[13] "Egamma Cut-Based Identification",. https://twiki.cern.ch/twiki/bin/view/CMS/EgammaCutBasedIdentification#Electron_ID_Working_Points.

[14] CMS Collaboration, "Data-Driven Estimation of the Invisible Z Background to the SUSY MET Plus Jets Search", CMS Physics Analysis Summary CMS-PAS-SUS-08-002, CERN, (2008).

[15] CMS Collaboration, "Performance of Methods for Data-Driven Background Estimation in SUSY Searches", CMS Physics Analysis Summary CMS-PAS-SUS-10-001, CERN, (2010).

[16] CMS Collaboration, "Search for supersymmetry in all-hadronic events with MT2", CMS Physics Analysis Summary CMS-PAS-SUS-11-005, CERN, (2011).

[17] CMS Collaboration, "Combination of b-tagging efficiency measurements in 2012 data at 8 TeV pp collision", CMS Physics Analysis Summary CMS-BTV-AN-12-470, CERN, (2012).

[18] A. L. Read., "Presentation of search results: the CLs technique.", *J.Phys.G: Nucl. Part. Phys.* **28** (2002).

[19] E. G. Glen Cowan, Kyle Cranmer and O. Vitells, "Asymptotic formulae for likelihood-based tests of new physics.", *Eur.Phys.J.* **C71:1554** (2011).

[20] "The RooStats-based statistics tools for Higgs PAG",. `https://twiki.cern.ch/twiki/bin/viewauth/CMS/SWGuideHiggsAnalysisCombinedLimit`.

[21] D.Alves et al., "Simplified Models for LHC New Physics Searches.", `arXiv:1105.2838`.

[22] T. S. W. G. for Hadronic Stops, "Search for Direct Scalar Top-quark Pair Production in the All-hadronic Channel at 8 TeV using a Top-quark tagger", CMS Analysis Note 2012/490, CERN, (2012).